OXFORD

Cerebral Cortex, 2023, **33**, 6207–6227
https://doi.org/10.1093/cercor/bhac496
Advance access publication date 27 December 2022
Original Article

Auditory cortical connectivity in humans

Edmund T. Rolls [1,2,6,*], Josef P. Rauschecker[3,8], Gustavo Deco[4,5], Chu-Chung Huang[6], Jianfeng Feng[2,7]

[1]Oxford Centre for Computational Neuroscience, Oxford, UK,
[2]Department of Computer Science, University of Warwick, Coventry CV4 7AL, UK,
[3]Department of Neuroscience, Georgetown University Medical Center, Washington, DC 20057, USA,
[4]Center for Brain and Cognition, Computational Neuroscience Group, Department of Information and Communication Technologies, Universitat Pompeu Fabra, Roc Boronat 138, Brain and Cognition, Pompeu Fabra University, Barcelona 08018, Spain,
[5]Institució Catalana de la Recerca i Estudis Avançats (ICREA), Universitat Pompeu Fabra, Passeig Lluís Companys 23, Barcelona 08010, Spain,
[6]Shanghai Key Laboratory of Brain Functional Genomics (Ministry of Education), School of Psychology and Cognitive Science, East China Normal University, Shanghai 200602, China,
[7]Institute of Science and Technology for Brain Inspired Intelligence, Fudan University, Shanghai 200403, China,
[8]Institute for Advanced Study, Technical University, Munich, Germany

*Corresponding author: Department of Computer Science, University of Warwick, Coventry CV4 7AL, UK. Email: Edmund.Rolls@oxcns.org

To understand auditory cortical processing, the effective connectivity between 15 auditory cortical regions and 360 cortical regions was measured in 171 Human Connectome Project participants, and complemented with functional connectivity and diffusion tractography. 1. A hierarchy of auditory cortical processing was identified from Core regions (including A1) to Belt regions LBelt, MBelt, and 52; then to PBelt; and then to HCP A4. 2. A4 has connectivity to anterior temporal lobe TA2, and to HCP A5, which connects to dorsal-bank superior temporal sulcus (STS) regions STGa, STSda, and STSdp. These STS regions also receive visual inputs about moving faces and objects, which are combined with auditory information to help implement multimodal object identification, such as who is speaking, and what is being said. Consistent with this being a "what" ventral auditory stream, these STS regions then have effective connectivity to TPOJ1, STV, PSL, TGv, TGd, and PGi, which are language-related semantic regions connecting to Broca's area, especially BA45. 3. A4 and A5 also have effective connectivity to MT and MST, which connect to superior parietal regions forming a dorsal auditory "where" stream involved in actions in space. Connections of PBelt, A4, and A5 with BA44 may form a language-related dorsal stream.

Key words: auditory cortex; ventral and dorsal auditory streams; effective connectivity; functional connectivity; diffusion tractography; language.

Introduction

To understand auditory cortical processing involved in hearing, speech, and language, it is important to understand the connectivity of human auditory cortical regions. The aim of the present investigation is to advance understanding of the connections and connectivity of the human cortical auditory pathways.

To do this, we measured with Human Connectome Project (HCP) data (Glasser et al. 2016b) the direct connections between brain regions using diffusion tractography; the functional connectivity between brain regions using the correlation between the BOLD signals in resting state fMRI, which provides evidence about the strength of interactions; and the effective connectivity, which provides evidence about the strength and direction of the causal connectivity between pairs of hundreds of brain regions with a new Hopf algorithm (Rolls et al. 2022f). These measures were made between the 360 cortical regions in the HCP multimodal parcellation atlas (HCP-MMP) (Glasser et al. 2016a). The HCP-MMP atlas provides the most detailed parcellation of the human cortical areas that we know, in that its 360 regions are defined using a combination of structural measures (cortical thickness and cortical myelin content), functional connectivity, and task-related fMRI (Glasser et al. 2016a). This parcellation is the parcellation of choice for the cerebral cortex because it is based on multimodal information (Glasser et al. 2016a) with the definition and boundaries set out in their Glasser_2016_SuppNeuroanatomy.pdf, and it is being used as the basis for many new investigations of brain function and connectivity, which can all be cast in the same framework (Colclough et al. 2017; Van Essen and Glasser 2018; Sulpizio et al. 2020; Yokoyama et al. 2021; Rolls et al. 2022e, 2022f, 2022g). This approach provides better categorization of cortical areas than does for example functional connectivity alone (Power et al. 2011). A summary of the boundaries, tractography, functional connectivity, and task-related activations of visual cortical areas using the HCP-MMP atlas is available elsewhere (Glasser et al. 2016a; Baker et al. 2018a, 2018b), but the effective connectivity, tractography, and functional connectivity analyses described here are new, and further are presented in quantitative form using connectivity matrices for all 360 cortical areas.

Previous understanding of cortical auditory information pathways has been founded on research in non-human primates supplemented by activation and functional connectivity studies in humans (Morel et al. 1993; Rauschecker et al. 1995; Rauschecker 1998a, 1998b; Romanski et al. 1999; Kaas and Hackett 2000; Rauschecker and Tian 2000; Poremba et al. 2003; Rauschecker and Scott 2009; DeWitt and Rauschecker 2012; Rauschecker 2012; Ahveninen et al. 2013; DeWitt and Rauschecker 2013; Kravitz et al. 2013; Fukushima et al. 2014; Kikuchi et al. 2014; Moerel et al. 2014; Scott et al. 2014; Karabanov et al. 2015; Munoz-Lopez et al. 2015; Petkov et al. 2015; Bornkessel-Schlesewsky et al. 2015a; DeWitt and Rauschecker 2016; Leaver and Rauschecker 2016; Scott and Mishkin 2016; Glasser et al. 2016a; Erickson et al. 2017; Scott et al. 2017; Van Essen and Glasser 2018; Rauschecker 2018a, 2018b; Corcoles-Parada et al. 2019; van der Heijden et al. 2019; Archakov et al. 2020). One perspective, with its foundations

Received: September 25, 2022. **Revised:** November 27, 2022. **Accepted:** November 29, 2022
© The Author(s) 2022. Published by Oxford University Press. All rights reserved. For permissions, please e-mail: journals.permission@oup.com.

Downloaded from https://academic.oup.com/cercor/article/33/10/6207/6960609 by University of Warwick user on 15 May 2023

in research on macaques, is that a ventral auditory pathway is involved in the decoding of spectrally complex sounds ("auditory objects"), which includes the decoding of speech sounds ("speech perception") and their ultimate linking to meaning in humans. An auditory dorsal pathway is involved in sensorimotor integration and control (Rauschecker 2011), and in humans plays a role in speech production as well as categorization of phonemes during speech processing (Rauschecker 2012). In more detail, in both humans and nonhuman primates, the auditory cortex is described as having core (corresponding to primary and primary-like auditory cortex), then belt (which surrounds the core), and then parabelt fields, all of which contain several subfields (Rauschecker 2015). Neurons in the core show responses with narrow tuning to tone frequency; belt neurons respond best to band-passed noise of a specific frequency and bandwidth; and parabelt neurons respond to increasingly complex sounds. The belt areas give rise to two major pathways, one that is anteroventrally directed and projects to ventrolateral prefrontal cortex and another that is posterodorsally directed and projects to dorsolateral prefrontal cortex. The ventral stream underlies auditory pattern and object recognition, including the decoding of speech sounds at the level of phonemes, words, and short phrases (Obleser et al. 2006). The dorsal stream is involved in the processing of auditory space and motion and is generally considered an audiomotor pathway for sensorimotor integration and control (Rauschecker 2011). As such, it is involved in functions of sentence processing, silent speech, and processing of musical sequences. Inferior parietal and premotor cortices are all part of this dorsal stream network (Rauschecker 2015). This perspective therefore is that the organization of the auditory cortical system resembles that of the visual cortical system in that it consists of two major pathways that fulfill two fundamentally different tasks in higher sensory and cognitive processing. As in vision, the debate whether there might be more than two processing streams began right after the initial discovery (Kaas and Hackett 1999; Belin and Zatorre 2000; Romanski et al. 2000). This discussion has been particularly intense in the discussion of language pathways, where debate about the origin of language is often ideologically fraught. While the existence of a direct projection from auditory to prefrontal regions along the auditory dorsal pathway is unquestionable in humans (the "arcuate" fasciculus (Geschwind 1970), evidence for its existence is somewhat sparser in monkeys, but still clearly apparent from anatomical tracer studies in physiologically identified cortical regions (Romanski et al. 1999) as well as high-resolution imaging (Frey et al. 2008). This quantitative difference has led some authors to suggest (on the basis of imaging data) that the origin of language may depend on the existence of a direct dorsal pathway (Rilling et al. 2011; Skeide and Friederici 2016), a claim that is no longer sustainable (Bornkessel-Schlesewsky et al. 2015b; Balezeau et al. 2020). Thus, the human data are entirely consistent with the monkey data (Romanski et al. 1999; Petrides and Pandya 2002, 2009; Frey et al. 2014) in demonstrating the distinct connectivity of the pars opercularis (area 44) versus the pars triangularis (area 45) that together constitute Broca's region (Friederici 2002; Amunts et al. 2010; Amunts and Zilles 2012; Friederici et al. 2017). More recent revelations about the dorsal stream show that it has presumably evolved as a substrate for sensorimotor processing, connecting sensory, and motor cortical systems with each other and the basal ganglia (Rauschecker 2018a; Archakov et al. 2020), thus permitting the learning of sequences and the origin of both language and music (Rauschecker 2018b).

The present research goes beyond this previous research by estimating causal connectivity between 15 auditory cortical regions in the human brain with a multimodal atlas with 360 cortical areas. Strengths of this investigation are that it utilized this HCP-MMP atlas (Glasser et al. 2016a); HCP data from the same set of 171 participants imaged at 7T (Glasser et al. 2016b) in whom we could calculate the connections, functional connectivity, and effective connectivity; and that it utilized a method for effective connectivity measurement between all 360 cortical regions investigated here. The Hopf effective connectivity algorithm is important for helping to understand the operation of the computational system, for it is calculated using time delays in the signals between 360 or more cortical regions (Rolls et al. 2022f, 2022g), and the use of time is an important component in the approach to causality (Rolls 2020, 2021a, 2021b). To facilitate comparison between different cortical systems and processing streams, the approach used here is similar to that used in investigations of other cortical regions (Huang et al. 2021; Ma et al. 2022; Rolls et al. 2022a, 2022b, 2022c, 2022d, 2022e, 2022f, 2022g, 2022h), with overviews of how these connectivity analyses provide a connectivity framework helpful for understanding brain computations provided by Rolls (2023b). We hope that future research using the same brain atlas (Glasser et al. 2016a; Huang et al. 2022) will benefit from the human auditory cortical connectome described here (Rolls 2022a).

Methods

Participants and data acquisition

Multiband 7T resting state functional magnetic resonance images (rs-fMRI) of 184 individuals were obtained from the publicly available S1200 release (last updated: April 2018) of the Human Connectome Project (HCP) (Van Essen et al. 2013), with data available for all the analyses including the tractography available in 171 participants (see below). Individual written informed content was obtained from each participant, and the scanning protocol was approved by the Institutional Review Board of Washington University in St. Louis, MO, USA (IRB #201204036).

Multimodal imaging was performed in a Siemens Magnetom 7T housed at the Center for Magnetic Resonance (CMRR) at the University of Minnesota in Minneapolis. For each participant, a total of four sessions of rs-fMRI were acquired, with oblique axial acquisitions alternated between phase encoding in a posterior-to-anterior (PA) direction in sessions 1 and 3, and an anterior-to-posterior (AP) phase encoding direction in sessions 2 and 4. Specifically, each rs-fMRI session was acquired using a multiband gradient-echo EPI imaging sequence. The following parameters were used: TR = 1000 ms, TE = 22.2 ms, flip angle = 45°, field of view = 208 × 208, matrix = 130 × 130, 85 slices, voxel size = 1.6 × 1.6 × 1.6 mm^3, multiband factor = 5. The total scanning time for the rs-fMRI protocol was approximately 16 min with 900 volumes. Further details of the 7T rs-fMRI acquisition protocols are given in the HCP reference manual (https://humanconnectome.org/storage/app/media/documentation/s1200/HCP_S1200_Release_Reference_Manual.pdf).

The current investigation was designed to complement investigations of effective and functional connectivity and diffusion tractography of the hippocampus (Huang et al. 2021; Ma et al. 2022; Rolls et al. 2022f), posterior cingulate cortex (Rolls et al. 2022h), orbitofrontal and anterior cingulate cortices (Rolls et al. 2022g), visual pathways (Rolls et al. 2022b), language regions (Rolls et al. 2022e), parietal cortex (Rolls et al. 2022d), and prefrontal and somatosensory cortex (Rolls et al. 2022a), and so the same 171 participants with data for the first session of rs-fMRI at 7T were used for the analyses described here (age 22–36 years, 66 males).

Downloaded from https://academic.oup.com/cercor/article/33/10/6207/6960609 by University of Warwick user on 15 May 2023

Data preprocessing

The preprocessing was performed by the HCP as described in Glasser et al. (2013), based on the updated 7T data pipeline (v3.21.0, https://github.com/Washington-University/HCPpipelines), including gradient distortion correction, head motion correction, image distortion correction, spatial transformation to the Montreal Neurological Institute space using one step spline resampling from the original functional images followed by intensity normalization. In addition, the HCP took an approach using ICA (FSL's MELODIC) combined with a more automated component classifier referred to as FIX (FMRIB's ICA-based X-noisifier) to remove non-neural spatiotemporal artifact (Smith et al. 2013; Griffanti et al. 2014; Salimi-Khorshidi et al. 2014). This step also used 24 confound timeseries derived from the motion estimation (6 rigid-body parameter timeseries, their backwards-looking temporal derivatives, plus all 12 resulting regressors squared (Satterthwaite et al. 2013) to minimize noise in the data. The preprocessing performed by the HCP also included boundary-based registration between EPI and T1w images, and brain masking based on FreeSurfer segmentation. The "minimally preprocessed" rsfMRI data provided by the HCP 1200 release (rfMRI*hp2000_clean.dtseries) were used in this investigation. The preprocessed data is in the HCP grayordinates standard space and is made available in a surface-based CIFTI file for each participant. With the MATLAB script (cifti toolbox: https://github.com/Washington-University/cifti-matlab), we extracted and averaged the cleaned timeseries of all the grayordinates in each region of the HCP-MMP 1.0 atlas (Glasser et al. 2016a), which is a group-based parcellation defined in the HCP grayordinate standard space having 180 cortical regions per hemisphere, and is a surface-based atlas provided in CIFTI format. The timeseries were detrended, and temporally filtered with a second order Butterworth filter set to 0.008–0.08 Hz.

Brain atlas and region selection

To construct the effective connectivity for the regions of interest in this investigation with other parts of the human brain, we utilized the 7T resting state fMRI data the HCP, and parcellated this with the surface-based HCP-MMP atlas, which has 360 cortical regions (Glasser et al. 2016a). We were able to use the same 171 participants for whom we also had performed diffusion tractography, as described in detail (Huang et al. 2021). The brain regions in this atlas (Glasser et al. 2016a) are shown in Fig. 1 and Supplementary Fig. S1, and a list of the cortical regions in this atlas is provided in Supplementary Table S1 in the reordered form used in the extended volumetric HCPex atlas (Huang et al. 2022).

The auditory cortical regions selected for connectivity analysis here were as follows, in the HCP-MMP division indicated as listed in Supplementary Table S1, and as illustrated in Fig. 1 and Supplementary Fig. S1. Early Auditory division: Area 52, A1 Primary Auditory Cortex, LBelt Lateral Belt Complex, MBelt Medial Belt Complex, PBelt ParaBelt Complex, PFcm (which is part of the parietal cortex), and RI RetroInsular Area. Auditory Association division: A4 Auditory 4 Complex, A5 Auditory 5 Complex, TA2, STGa, STSda Area STS dorsal anterior, STSdp Area STS dorsal posterior, STSva Area STS ventral anterior, and STSvp Area STS ventral posterior. It is noted that the HCP-MMP atlas sometimes uses dorsal vs ventral as descriptors following nomenclature in non-human primates, and that these correspond to superior and inferior in humans. For those becoming familiar with the HCP-MMP atlas, in the name of a brain region typically a = anterior, p = posterior, d = dorsal (i.e. superior in the human brain), v = ventral (i.e. inferior in the human brain), m = medial, l or L = lateral, T = temporal, P = parietal, and V = visual. It must also be noted that some of the names used in the HCP-MMP atlas utilize the name of the corresponding region in macaques, but in humans, the cortical region may not be topologically in the same place (e.g. sulcus) as in macaques.

The parcellation of the auditory cortical divisions in the HCP-MMP atlas and the evidence for the boundaries of the different regions are provided by Glasser et al. (2016a) in their Supplementary Material file Glasser_2016_SuppNeuroanatomy.pdf.

Measurement of effective connectivity

Effective connectivity measures the effect of one brain region on another and utilizes differences detected at different times in the signals in each connected pair of brain regions to infer effects of one brain region on another. One such approach is dynamic causal modeling, but it applies most easily to activation studies, and is typically limited to measuring the effective connectivity between just a few brain areas (Friston 2009; Valdes-Sosa et al. 2011; Bajaj et al. 2016), though there have been moves to extend it to resting state studies and more brain areas (Frassle et al. 2017; Razi et al. 2017). The method used here (see Rolls et al. 2022f, 2022g) was developed from a Hopf algorithm to enable measurement of effective connectivity between many brain areas, described by Deco et al. (2019). A principle is that the functional connectivity is measured at time t and time $t + tau$, where tau is typically 2 s to take into account the time within which a change in the BOLD signal can occur, and that tau should be short to capture causality, and then the effective connectivity model is trained by error correction until it can generate the functional connectivity matrices at time t and time $t + tau$. Further details of the algorithm, and the development that enabled it to measure the effective connectivity in each direction, are described next and in more detail in the Supplementary Material.

To infer the effective connectivity, we use a whole-brain model that allows us to simulate the BOLD activity across all brain regions and time. We use the so-called Hopf computational model, which integrates the dynamics of Stuart-Landau oscillators, expressing the activity of each brain region, by the underlying anatomical connectivity (Deco et al. 2017b). As mentioned above, we include in the model 360 cortical brain areas (Huang et al. 2022). The local dynamics of each brain area (node) is given by Stuart-Landau oscillators, which expresses the normal form of a supercritical Hopf bifurcation, describing the transition from noisy to oscillatory dynamics (Kuznetsov 2013). During the last years, numerous studies were able to show how the Hopf whole-brain model successfully simulates empirical electrophysiology (Freyer et al. 2011, 2012), MEG (Deco et al. 2017a), and fMRI (Kringelbach et al. 2015; Deco et al. 2017b; Kringelbach and Deco 2020).

The Hopf whole-brain model can be expressed mathematically as follows:

$$\frac{dx_i}{dt} = \overbrace{\left[a_i - x_i^2 - y_i^2\right]x_i - \omega_i y_i}^{Local\ Dynamics} + \overbrace{G\sum_{j=1}^{N} C_{ij}\left(x_j - x_i\right)}^{Coupling} + \overbrace{\beta\eta_i(t)}^{Gaussian\ Noise} \quad (1)$$

$$\frac{dy_i}{dt} = \left[a_i - x_i^2 - y_i^2\right]y_i + \omega_i x_i + G\sum_{j=1}^{N} C_{ij}\left(y_j - y_i\right) + \beta\eta_i(t) \quad (2)$$

Downloaded from https://academic.oup.com/cercor/article/33/10/6207/6960609 by University of Warwick user on 15 May 2023

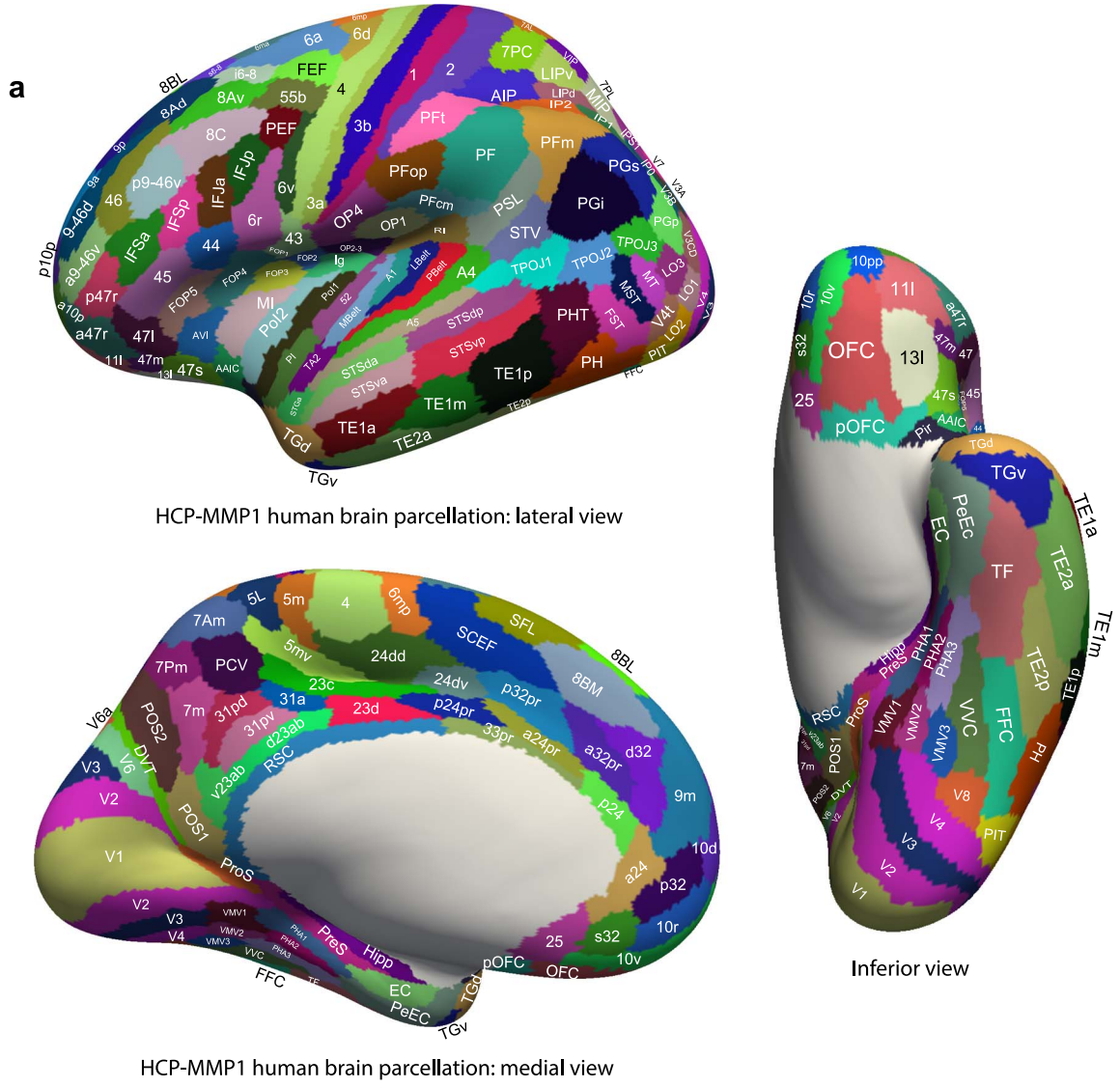

Fig. 1a. Anatomical regions of the human visual and other cortical regions. Regions are shown as defined in the HCP-MMP atlas (Glasser et al. 2016a), and in its extended version HCPex (Huang et al. 2022). The regions are shown on images of the human brain with the sulci expanded sufficiently to allow the regions within the sulci to be shown. Supplementary Figs. S1-S7 Shows the brain without the sulci opened to help show which regions/areas are normally visible. Abbreviations are provided in Supplementary Table S1.

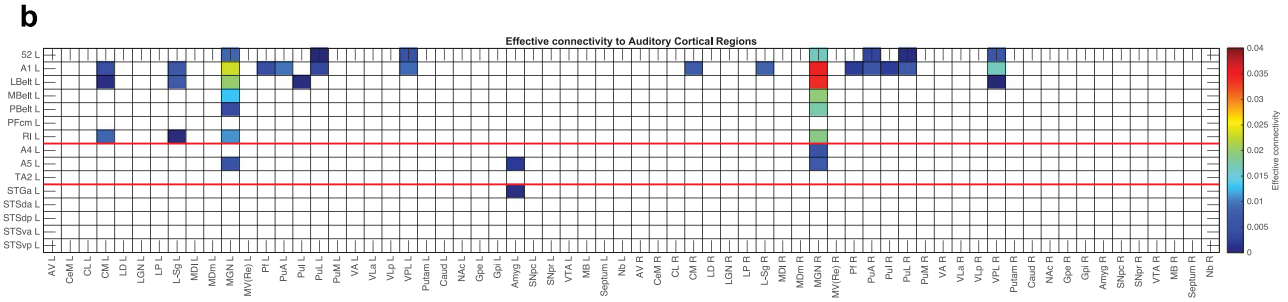

Fig. 1b. Subcortical connectivity of auditory cortical regions. The effective connectivity of auditory cortex regions in the left hemisphere. The connectivity is read from column to row. L = left; R = right; CM = central median nucleus of the thalamus; L-sg = Limitans Suprageniculate of the thalamus; MGN = medial geniculate nucleus; pf = Parafascicular nucleus of the thalamus; PuA = Pulvinar anterior; PuI = Pulvinar inferior; PuL = Pulvinar lateral; VPL = ventrolateral nucleus of the thalamus; Amyg = amygdala. The abbreviations for the cortical regions (the rows) are in Supplementary Table S1, and the abbreviations for the subcortical regions are in Supplementary Table S2. The regions above the upper red line are in the HCP-MMP "early auditory" division; between the two red lines are in the "auditory association" division; and below the lower red line are for the cortex in and related to the superior temporal sulcus (STS). This analysis was performed using the subcortical regions defined in the HCPex atlas (Huang et al. 2022).

Downloaded from https://academic.oup.com/cercor/article/33/10/6207/6960609 by University of Warwick user on 15 May 2023

Equations 1 and 2 describe the coupling of Stuart-Landau oscillators through an effective connectivity matrix C. The $x_i(t)$ term represents the simulated BOLD signal data of brain area *i*. The values of $y_i(t)$ are relevant to the dynamics of the system but are not part of the information read out from the system. In these equations, $\eta_i(t)$ provides additive Gaussian noise with standard deviation β. The Stuart-Landau oscillators for each brain area *i* express a Hopf normal form that has a supercritical bifurcation at a_i=0, so that if $a_i > 0$ the system has a stable limit cycle with frequency $f_i=\omega_i/2\pi$ (where ω_i is the angular velocity); and when $a_i < 0$, the system has a stable fixed point representing a low activity noisy state. The intrinsic frequency f_i of each Stuart-Landau oscillator corresponding to a brain area is in the 0.008–0.08 Hz band (i = 1, …, 360). The intrinsic frequencies are fitted from the data, as given by the averaged peak frequency of the narrowband BOLD signals of each brain region. The coupling term representing the input received in node *i* from every other node *j*, is weighted by the corresponding effective connectivity C_{ij}. The coupling is the canonical diffusive coupling, which approximates the simplest (linear) part of a general coupling function. *G* denotes the global coupling weight, scaling equally the total input received in each brain area. While the oscillators are weakly coupled, the periodic orbit of the uncoupled oscillators is preserved. Details are provided in the Supplementary Material.

The effective connectivity matrix is derived by optimizing the conductivity of each existing anatomical connection as specified by the Structural Connectivity matrix (measured with tractography (Huang et al. 2021)) in order to fit the empirical functional connectivity (FC) pairs and the lagged FC^{tau} pairs. By this, we are able to infer a non-symmetric Effective Connectivity matrix (see Gilson et al. (2016)). Note that FC^{tau}, ie the lagged functional connectivity between pairs, lagged at *tau* s, breaks the symmetry and thus is fundamental for our purpose. Specifically, we compute the distance between the model FC simulated from the current estimate of the effective connectivity and the empirical data FC^{emp}, as well as the simulated model FC^{tau} and empirical data FC^{tau_emp} and adjust each effective connection (entry in the effective connectivity matrix) separately with a gradient-descent approach. The model is run repeatedly with the updated effective connectivity until the fit converges towards a stable value.

We start with the anatomical connectivity obtained with probabilistic tractography from dMRI (or from an initial zero *C* matrix as described in the Supplementary Material) and use the following procedure to update each entry C_{ij}in the effective connectivity matrix

$$C_{ij} = C_{ij} + \varepsilon \left(FC_{ij}^{emp} - FC_{ij} + FC_{ij}^{tau\_emp} - FC_{ij}^{tau} \right) \quad (3)$$

where ϵ is a learning rate constant, and *i* and *j* are the nodes. When updating each connection if the initial matrix is a dMRI structural connection matrix (see Supplementary Material), the corresponding link to the same brain regions in the opposite hemisphere is also updated, as contralateral connections are not revealed well by dMRI. The convergence of the algorithm is illustrated by Rolls et al. (2022f), and the utility of the algorithm was validated as described below.

For the implementation, we set *tau* to be 2 s, selecting the appropriate number of TRs to achieve this. The maximum effective connectivity was set to a value of 0.2, and was found between V1 and V2.

Effective connectome

Whole-brain effective connectivity (EC) analysis was performed between the 15 auditory cortical regions described above (see Fig. 1 and Supplementary Fig. S1) and the 360 regions defined in the surface-based HCP-MMP atlas (Glasser et al. 2016a) in their reordered form provided in Supplementary Table S1, described in the Supplementary material, and used in the volumetric extended HCPex atlas (Huang et al. 2022). This EC was computed for all 171 participants. The effective connectivity algorithm was run until it had reached the maximal value for the correspondence between the simulated and empirical functional connectivity matrices at time *t* and *t*+*tau* (see Supplementary Material). The effective connectivity calculated was checked and validated in a number of ways described in the Supplementary Material.

To test whether the vectors of effective connectivities of each of the 15 auditory cortex regions with the 180 areas in the left hemisphere of the modified HCP atlas were significantly different, the interaction term was calculated for each pair of the 15 auditory cortex regions effective connectivity vectors in separate two-way ANOVAs (each 2 × 180) across the 171 participants, and Bonferroni correction for multiple comparisons was applied.

Functional connectivity

For comparison with the effective connectivity, the functional connectivity was also measured at 7T with the identical set of participants, data, and filtering of 0.008–0.08 Hz. The functional connectivity was measured by the Pearson correlation between the BOLD signal timeseries for each pair of brain regions, and is in fact the FC^{emp} referred to above. A threshold of 0.4 is used for the presentation of the findings in Fig. 5; for this sets, the sparseness of what is shown to a level commensurate with the effective connectivity, to facilitate comparison between the functional and the effective connectivity. The functional connectivity can provide evidence that may relate to interactions between brain regions, while providing no evidence about causal direction-specific effects. A high functional connectivity may in this scenario thus reflect strong physiological interactions between areas, and provides a different type of evidence to effective connectivity. The effective connectivity is non-linearly related to the functional connectivity, with effective connectivities being identified (i.e. greater than zero) only for the links with relatively high functional connectivity.

Connections shown with diffusion tractography

Diffusion tractography can provide evidence about fiber pathways linking different brain regions with a method that is completely different to the ways in which effective and functional connectivity are measured, so is included here to provide complementary and supporting evidence to the effective connectivity. Diffusion tractography shows only direct connections, so comparison with effective connectivity can help to suggest which effective connectivities may be mediated directly or indirectly. Diffusion tractography does not provide evidence about the direction of connections. Diffusion tractography was performed on the same 171 HCP participants imaged at 7T with methods described in detail elsewhere (Huang et al. 2021). The major parameters were 1.05 mm isotropic voxels; a two- shell acquisition scheme with *b*-values = 1000, 2000 s/mm^2, repetition time/echo time = 7000/71 ms, 65 unique diffusion gradient directions and 6 b0 images obtained for each phase encoding direction pair (AP and PA pairs). Pre-processing steps included distortion correction, eddy-current correction, motion correction, and gradient non-linearity correction. In brief, whole brain tractography was reconstructed for each subject in native space. To improve the tractography termination accuracy in GM, MRtrix3's 5ttgen command was used to generate multi-tissue segment images (5tt)

Downloaded from https://academic.oup.com/cercor/article/33/10/6207/6960609 by University of Warwick user on 15 May 2023

using T1 images, the segmented tissues were then co-registered with the b0 image in diffusion space. For multi-shell data, tissue response functions in GM, WM, and CSF were estimated by the MRtrix3' dwi2response function with the Dhollander algorithm (Dhollander et al. 2016). A Multi-Shell Multi-Tissue Constrained Spherical Deconvolution (MSMT-CSD) model with lmax = 8 and prior co-registered 5tt image was used on the preprocessed multi-shell DWI data to obtain the fiber orientation distribution (FOD) function (Smith 2002; Jeurissen et al. 2014). Based on the voxel-wise fiber orientation distribution, anatomically constrained tractography (ACT) using the probabilistic tracking algorithm: iFOD2 (second-order integration based on FOD) with dynamic seeding was applied to generate the initial tractogram (1 million streamlines with maximum tract length = 250 mm and minimal tract length = 5 mm). To quantify the number of streamlines connecting pairs of regions, the updated version of the spherical-deconvolution informed filtering of the tractograms (SIFT2) method was applied, which provides more biologically meaningful estimates of structural connection density (Smith et al. 2015). The SIFT2 algorithm weighted the streamlines number based on the overall distribution of fiber orientation distribution function across voxels (Unlike the regular SIFT algorithm that filters streamlines from a great number to a much smaller number to reduce reconstruction biases of streamline tractography, the SIFT2 algorithm utilizes all input streamlines and applies weighting to them. In this case, the total number of reconstructed streamlines remains unmodified.)

The results for the tractography are shown in Fig. 6 as the number of streamlines between areas with a threshold applied of 10 to reduce the risk of occasional noise-related observations. The highest level in the color bar was set to 1000 streamlines between a pair of cortical regions in order to show graded values for a number of links. The term "connections" is used when referring to what is shown with diffusion tractography, and connectivity when referring to effective or functional connectivity.

Results

Overview: effective connectivity, functional connectivity, and diffusion tractography

The effective connectivities to the 15 auditory cortical regions from other cortical regions in the left hemisphere are shown in Fig. 2. The effective connectivities from the 15 auditory cortical regions to other cortical regions in the left hemisphere are shown in Fig. 3. The vectors of effective connectivities of each of the 15 auditory cortical regions with the 180 regions in the left hemisphere of the HCP-MMP atlas were all significantly different from each other (Across the 171 participants, the interaction term in separate two-way ANOVAs for the comparisons between the effective connectivity of every pair of the 15 auditory cortical ROIs after Bonferroni correction for multiple comparisons were all $P < 10^{-90}$.) The results were confirmed with the non-parametric Scheirer-Ray-Hare test (Scheirer et al. 1976; Sinha 2022). The connectivity of each of the auditory cortical regions is considered in the section Results in the order shown in Supplementary Table S1, except that region TA2 was moved before the STS regions as their connectivity is somewhat different. The effective connectivities described in the text are the stronger ones, typically >0.01, but all of those greater than 0 are shown in the figures. The functional implications of the results described next are considered in the section Discussion. Figure 7 and b may be useful to provide a schematic overview of the auditory system connectivity in humans, though the quantitative details are provided in Figs. 2-4 considered in the section Results.

Subcortical connectivity of auditory cortical regions

The subcortical connectivity of the 15 auditory cortex regions is shown in Fig. 1b using the subcortical regions defined in the HCPex atlas (Huang et al. 2022). The left (L) medial geniculate, the main thalamic auditory nucleus, has the strongest effective connectivity to A1 (0.023 L, 0.026 R), then LBelt (0.020 L, 0.022 R), and then MBelt (0.013 L, 0.012 R), RI (0.011 L, 0.007 R), 52 (0.009 L, 0.006 R), and A5 (0.006 L, 0.000 R). Thus, for A1, the connectivity was somewhat stronger from the contralateral medial geniculate, but this was not generally the case. Very interestingly, no effective connectivity was found from these auditory cortical regions to the medial geniculate, so the anatomical connections demonstrated in macaques seem to have low efficacy. Area 52 has subcortical connectivity similar to A1 (Fig. 1b), consistent with the likelihood that A52—present in humans and described by the HCP-MMP as a "transitional" area (Glasser et al. 2016a)—is at least at an early stage of cortical processing. Some weak effects from non-specific thalamic nuclei such as CM and parafascicular (shown in Supplementary Fig. S1 (Huang et al. 2022)) were found, as were some inputs from parts of the pulvinar to A1, LBelt, and 52 and from the amygdala to A5 and STGa (Fig. 1b).

The main auditory cortex regions with relatively strong effective connectivity from the medial geniculate were thus A1 (perhaps corresponding to BA41), 52, LBelt (just posterior to A1 see Fig. 1, and perhaps corresponding to BA42), and MBelt (just anterior to A1 in humans). In the macaque, in which three subdivisions of the medial geniculate are distinguished (MGv, MGd, and MGm), MGv projects to the core regions (A1 and the rostral auditory area R), whereas MGd and MGm project to the belt regions (LBelt and MBelt) (Rauschecker et al. 1997). Whether the same is true for humans is an open question.

Connectivity of regions in the Early Auditory division: 52, A1, LBelt, MBelt, PBelt, PFcm and RI

A1

Figure 2 shows that A1, which may correspond to BA41 and is a primary or core auditory region (together with areas R and RT in macaques) (Hackett et al. 2001; Moerel et al. 2014), has strongest effective connectivity to MBelt and LBelt regions (both 0.090), followed by PBelt (0.066) and RI (0.063). The connectivity from A1 was weaker to A4 and to TA2. In all cases, the connectivity is a little stronger in this direction than the reverse, consistent with the hypothesis that these are feedforward projections. The connectivity with region 52 is different, in that 52 connects more strongly to A1 (0.065) than vice versa (0.044). The directionality of these effective connectivities is brought out in Fig. 4.

What was less expected about A1 is that it also has some effective connectivity from V1-V3 (but not the reverse), and from some somatosensory regions (OP2-OP3, and supracallosal anterior cingulate cortex a24pr, p24pr, a32pr (Rolls et al. 2022g)). In addition, A1 has weak effective connectivity with PIT, STV and TPOJ3, posterior cingulate PCV and RSC, anterior cingulate regions, pOFC and p10p (Fig. 2).

Area 52

Area 52 is a transitional region (Glasser et al. 2016a) not known in macaques that may be an early auditory cortex region in humans, given its relatively strong inputs from the medial

Downloaded from https://academic.oup.com/cercor/article/33/10/6207/6960609 by University of Warwick user on 15 May 2023

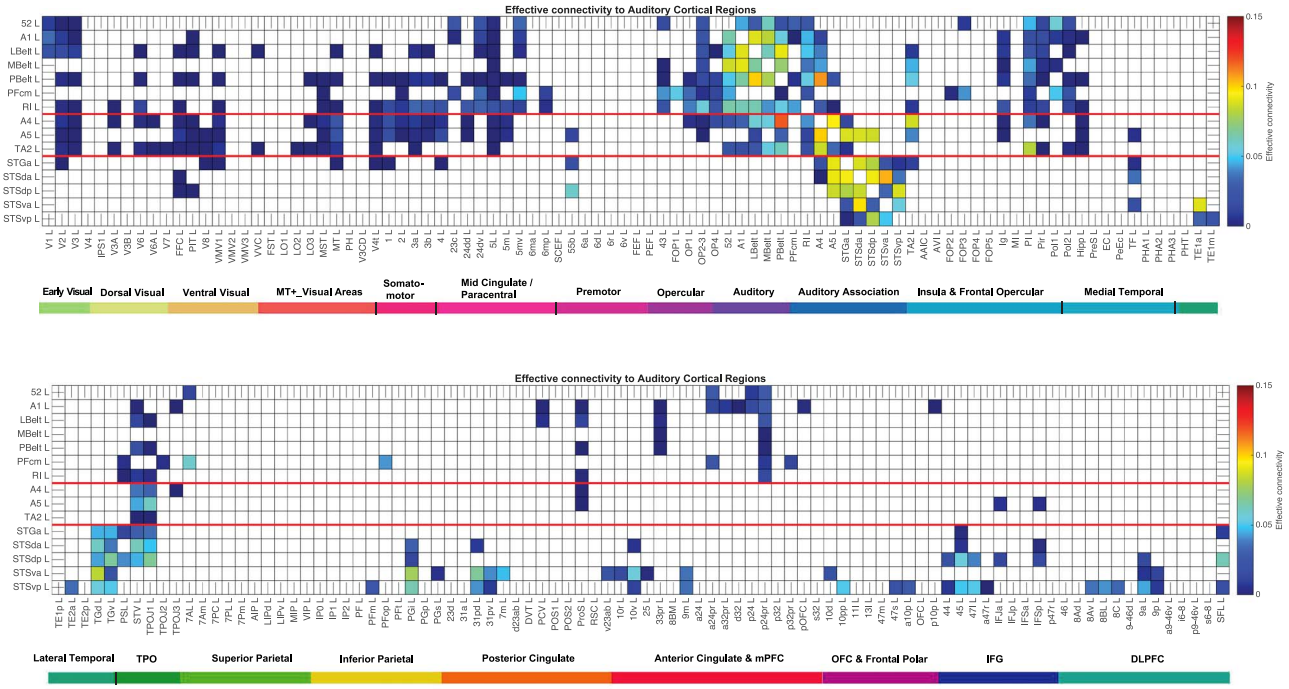

Fig. 2. Effective connectivity *TO* auditory cortical regions (the rows) *FROM* 180 cortical areas (the columns) in the left hemisphere. The effective connectivity is read from column to row. Effective connectivities of 0 are shown as blank. All effective connectivity maps are scaled to show 0.15 as the maximum, as this is the highest effective connectivity found between this set of brain regions. The effective connectivity color scale has been set to have a maximum of 0.15 as that is the range for the auditory regions, with the maximum value of 0.2 set by the connectivity between V1L and V2L. The regions above the upper red line are in the HCP-MMP "early auditory" division; between the two red lines are in the "auditory association" division; and below the lower red line are for the cortex in and related to the superior temporal sulcus (STS). The effective connectivity for the first set of cortical regions is shown in the top panel; and for the second set of regions in the lower panel. Abbreviations: See Supplementary Table S1. The colored labeled bars show the cortical divisions in the HCP-MMP atlas (Glasser et al. 2016a). The order of the cortical regions is that in Huang, Rolls et al (2022).

geniculate nucleus and the similarity of its thalamic inputs to those of A1 (Fig. 1b). Figure 2 shows that Area 52, which might be a medial belt area (Kusmierek and Rauschecker 2009; Moerel et al. 2014), has effective connectivity directed towards more strongly than the reverse in this order to the following: MBelt = 0.086, A1 = RI = 0.065, LBelt = PBelt = 0.051, PFcm = 0.044, A4 = TA2 = 0.020 (Figs. 2-4). Thus, although area 52 has weaker EC from the medial geniculate than A1, it does in its forward onward connectivity and weaker back-projections have similarity with the core auditory cortex region A1. In addition, Area 52 also has effective connectivity with a number of somatosensory cortical regions including 5mv, OP1-OP3, and insular regions PI, Ig, and PoI1-PoI2.

LBelt

LBelt has strong reciprocal effective connectivity with A1 and PBelt (>0.09), and moderate with MBelt, RI, and A4 (~0.06). It has some effective connectivity stronger in the forward direction to auditory association regions A5 and TA2. It receives from Area 52. LBelt has only relatively weak effective connectivity with somatosensory regions, and is different from A1 and Area 52 in this respect. LBelt has some effective connectivity from V1 and V2 (Fig. 2). It is noted that LBelt and MBelt each consist of 3 subdivisions (AL, ML, and CL for LBelt; AM, MM, and CM for the MBelt), identified by single-neuron mapping in the macaque (Rauschecker et al. 1995; Kusmierek and Rauschecker 2009). This may have consequences for the assignment of LBelt and MBelt regions to processing streams.

MBelt

MBelt has moderately strong reciprocal effective connectivity with A1 and PBelt (~0.08), moderate with LBelt and Area 52 (>0.06), and has connectivity that is stronger to auditory association areas A4 and TA2 (~0.055) than in the reverse direction (~0.045). In contrast to the auditory regions already described, it has no connectivity from visual areas such as V1-V3, and little somatosensory connectivity (with some mainly with para-insula region PI).

PBelt

PBelt has strong reciprocal effective connectivity with LBelt and MBelt (0.075–0.010), moderate with A1, RI and from Area 52 (~0.05), and has connectivity that is reciprocal and strong with auditory association A4 (>0.1), moderate with TA2 (>0.054), and also towards A5 (Figs. 2 and 3). It has only weak effective connectivity (<0.01) with visual and somatosensory regions. It has some effective connectivity with STV (0.015). Like LBelt, MBelt has also been subdivided on the basis of single-unit mapping, microanatomy and histochemistry into rostral and caudal subdivisions (RPB and CPB; (Hackett et al. 1999; Kaas and Hackett 2000; Kusmierek and Rauschecker 2009)), with (possibly severe) consequences for their assignment to processing streams (Tian et al. 2001).

PFcm

PFcm is a part of the inferior parietal cortex that has effective connectivity with auditory cortical regions especially RI and is included in the auditory division of the HCP-MMP atlas.

Downloaded from https://academic.oup.com/cercor/article/33/10/6207/6960609 by University of Warwick user on 15 May 2023

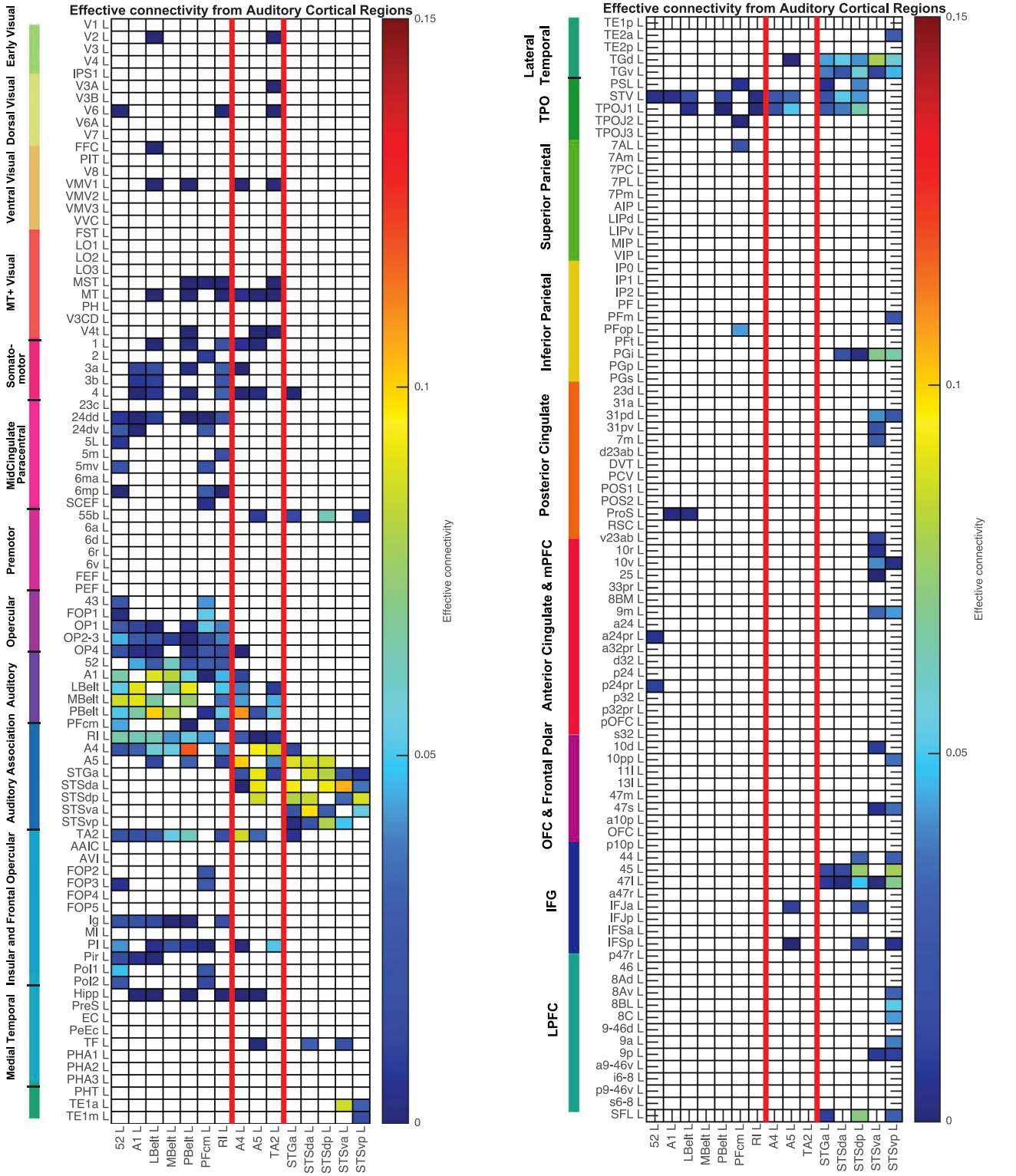

Fig. 3. Effective connectivity *FROM* the auditory cortical regions *TO* 180 cortical areas in the left hemisphere. The effective connectivity is read from column to row. Effective connectivities of 0 are shown as blank. Abbreviations: See Supplementary Table S1. The groups of auditory cortex regions are separated by red lines. Conventions as in Fig. 2.

PFcm receives from Area 52 (0.044 vs 0.030 in the reverse direction), and has effective connectivity to RI (0.043 vs 0.019 in the reverse direction). PFcm is however part of the inferior parietal cortex somatosensory processing hierarchy (Rolls et al. 2022d), and has extensive connectivity with somatosensory cortical regions including 5mv, FOP1-FOP3, OP1, and PoI1-PoI2 (It is relevant that somatosensory information is used in audio-motor learning for speech (Ohashi and Ostry 2021)). It has moderate connectivity with another part of the inferior parietal somatosensory hierarchy, PFop. It also receives from 7AL. PFcm may thus provide a route for auditory information to reach the inferior parietal cortex. The ventral intraparietal region

Downloaded from https://academic.oup.com/cercor/article/33/10/6207/6960609 by University of Warwick user on 15 May 2023

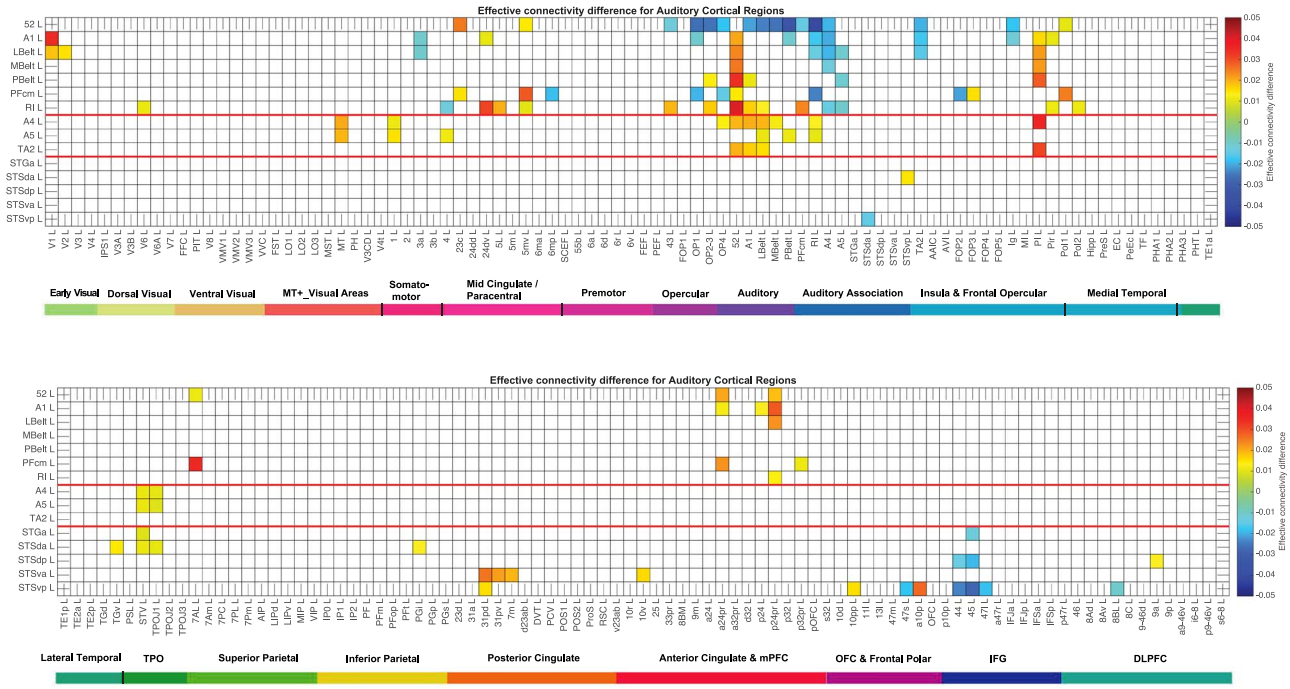

Fig. 4. Difference of the effective connectivity for auditory cortical regions with other cortical regions. For a given link, if the effective connectivity difference is positive, the connectivity is stronger in the direction from column to row. For a given link, if the effective connectivity difference is negative, the connectivity is weaker in the direction from column to row. This is calculated from 171 participants in the HCP imaged at 7T. the threshold value for any effective connectivity difference to be shown is 0.01. The color scale shows effective connectivity differences in the range −0.05 to +0.05. The abbreviations for the brain regions are shown in Supplementary Table S1, and the brain regions are shown in Fig. 1 and Supplementary Fig. S1. The effective connectivity difference for the first set of cortical regions is shown in the top panel; and for the second set of regions in the lower panel. Conventions as in Fig. 2.

(VIP) in the intraparietal sulcus (IPS) has been shown to receive anatomical input from auditory-related regions (Lewis and Van Essen 2000).

RI

RI, a retroinsular region, has moderate effective connectivity with auditory regions A1, 52, LBelt, MBelt, and Pbelt, and has connectivity directed towards auditory association A4, A5, and TA2. RI also has marked effective connectivity with somatosensory regions including 3a, 3b, 5 m, and OP1-OP4.

Connectivity of regions in the Auditory Association division: A4, A5 and TA2

A4

A4 receives effective connectivity strongly from PBelt (0.118), with some from MBelt and LBelt (~0.055), RI (0.041), and less from A1 (0.031) and area 52 (0.019) (Figs. 2 and 3) with the latter two quite directional (Fig. 4). A4 has strong reciprocal effective connectivity with A5 and TA2 (~0.09) and some with STGa (~0.015). A4 also receives from MT, rather weakly from some somatosensory regions apart from PI, which is stronger (Figs. 2-4), and has effective connectivity with language-related regions STV and TPOJ1 (see Rolls et al. (2022e)).

A5

A5 has very different connectivity to the preceding regions. A5 has its strongest effective connectivity with another auditory association region, A4 (~0.1), some with TA2 (~0.04), and less with earlier cortical regions, which instead of being from A1 and 52, are from PBelt and LBelt, suggesting that A5 is at a higher hierarchical position than A4. A5 in addition now has strong reciprocal effective connectivity with some STS and related regions, in particular STGa, STSda, and STSdp (~0.09). There is also some connectivity with STV and TPOJ1, which are language-related semantic regions (Rolls et al. 2022e). There is only rather weak effective connectivity from some somatosensory regions.

TA2

TA2 receives its strongest effective connectivity from A4 (~0.09), with moderate effective connectivity from MBelt, PBelt, and A5 (~0.05), and less and very directional from A1 and 52 (Figs. 2-4). It also receives from the parainsular PI. It has only a weak effective connectivity to STGa (0.01).

Superior Temporal Sulcus cortical regions: STGa, STS dorsal anterior STSda, STS dorsal posterior STSdp, STS ventral anterior STSva, STS ventral posterior STSvp

STGa

STGa receives much more strongly from A5 (0.1) than from A4 (0.017) or TA2 (0.010). STGa has strong effective connectivity with STSda and STSdp (~0.09). However, STGa has in addition moderate effective connectivity with the temporal pole, TGd and TGv (~0.045). It also has effective connectivity with STV and TPOJ1, and to a lesser extent with the PeriSylvian Language region PSL, all of which are language-related, semantic regions (Rolls et al. 2022e).

STGa also has effective connectivity to some regions that are output regions for language (Rolls et al. 2022e), Broca's area 45,

Downloaded from https://academic.oup.com/cercor/article/33/10/6207/6960609 by University of Warwick user on 15 May 2023

47 l, the Superior Frontal Language region SFL, and premotor 55b (Figs. 2-4).

More generally, STGa in the superior temporal gyrus at the temporal pole has strong connectivity with STSda, STSdp (which themselves have some connectivity with visual motion regions) and weaker with STSva. STGa also has effective connectivity with auditory regions A5, A4, and TA2 (but stronger with A5). It also has connectivity with language-related regions in the temporal pole (TGd and TGv) and in temporo-parieto-occipital regions PSL, STV, and TPOJ1; with the Superior Frontal Language area SFL; and with 55b. STGa connects to part of Broca's area, area 45 (Figs. 2-4). STGa is proposed to be part of a superior (i.e. anatomically dorsal) bank of the STS cortex semantic system including STSda and STSdp, which is involved in multimodal auditory and corresponding visual motion information (Rolls et al. 2022e).

STSda

STSda receives EC from A5 and STGa (and no earlier auditory cortex region, speaking to strong neighborhood relations) (though the connectivity is relatively strong in the reverse direction, and has strong reciprocal connectivity with STSdp and STSva (~0.095)). It has moderate EC with TGd, and language regions STV and TPOJ1. This region is novel in the hierarchy in receiving from the inferior parietal cortex PGi (0.03). It has some effective connectivity to part of Broca's area, 45 (Figs. 2-4).

STSda also has connectivity with parahippocampal TF, which provides inputs to the hippocampus (Rolls 2022b; Rolls et al. 2022f), and with a memory-related part of the posterior cingulate cortex (31pd) (Rolls et al. 2022h).

STSdp

STSdp in the cortex in the dorsal posterior part of the superior temporal sulcus has strong effective connectivity with A5, STGa, and STSda (and no earlier auditory cortex region).

STSdp also receives from parietal cortex region PGi, which has ventral temporal lobe visual and other connectivity (Rolls et al. 2022b, 2022d). It also has connectivity with language-related regions in the temporal pole (TGd and TGv), in temporo-parieto-occipital areas PSL, STV, and TPOJ1; with SFL; and with a left lateral orbitofrontal cortex region 47 l, which is also part of the language network (Rolls et al. 2022e). STSdp connects to Broca's area, strongly to 45 and less to 44 (Fig. 3), and to language-related parts of the inferior frontal gyrus IFJa and IFSp (Figs. 2-4). This connectivity provides evidence that STSdp is part of a superior (anatomically dorsal) STS semantic network with auditory and visual components (Rolls et al. 2022e).

STSva

STSva in the ventral anterior bank of the superior temporal sulcus has connectivity with other STS regions from which it may receive auditory information; receives strong visual effective connectivity from inferior temporal visual cortex TE1a in the object-related ventral visual stream (VVS); and it also receives strongly from inferior parietal visual region PGi, which has connectivity with ventral stream regions such as the inferior temporal visual cortex (Rolls et al. 2022b, 2022d) (Figs. 2-4). STSva has strong effective connectivity with STSda and TGd, and moderate with STGa, STSdp, STSvp. STSva has moderate effective connectivity with the hippocampal system via parahippocampal TF and the posterior cingulate cortex' memory-related regions 31pd, 31 pv, v23ab, and the related medial parietal 7 m (Rolls et al. 2022h). It also has effective connectivity with the reward-related ventromedial prefrontal cortex (vmPFC) 10v and pregenual anterior cingulate cortex 9 m, and this provides a route for auditory as well as visual information to reach the orbitofrontal/ventromedial prefrontal cortex (Rolls et al. 2022g) in which neuronal responses to face expression, head and face gesture, and vocalization are found (Rolls et al. 2006), and damage to which impairs emotional responses to these visual and auditory stimuli in humans (Rolls et al. 1994; Hornak et al. 1996; Hornak et al. 2003; Rolls 2014, 2023a). STSva is thus part of an inferior (ventral) bank STS semantic network (Rolls et al. 2022e).

STSvp

STSvp in the ventral posterior bank of the superior temporal sulcus has connectivity with other STS regions from which it may receive auditory information; it receives strong visual effective connectivity from object-related VVS inferior temporal visual cortex TE1a, TE1m, TE2a; and it also receives strongly from inferior parietal visual regions PGi and PFm, which connect with inferior temporal cortex VVS regions (Rolls et al. 2022d) (Figs. 2-4). It has strong effective connectivity with STSdp and STSva, and moderate with STSda, STSvp; and TGv and TGd. STSvp has some effective connectivity with the hippocampal system via the posterior cingulate cortex memory-related regions 31pd and 31 pv (Rolls et al. 2022h). It also has effective connectivity with the reward-related ventromedial prefrontal cortex 10v and pregenual anterior cingulate cortex 9 m. It also has effective connectivity to language-related areas 45, 44, 47 s, and 47r on the left and with the Superior Frontal Language region SFL, and premotor 55b (Rolls et al. 2022e). STSvp also has effective connectivity with dorsolateral prefrontal cortex short-term memory/visual attention-related regions 8Av, 8BL, 8C, and 9a, which have connectivity with the dorsal visual system (Rolls et al. 2022a). It is therefore proposed that STSvp is part of a ventral bank STS cortex semantic system (including visual input from the inferior temporal visual cortex, and parietal visual areas PGi and PFm associated with ventral-stream processing (Rolls et al. 2022d), and links this semantic system with outputs to Broca's area (especially 45, see Fig. 3) that are implicated in syntax (Friederici et al. 2017; Rolls et al. 2022e).

Effective connectivities of the 15 auditory cortical regions with contralateral cortical regions

The effective connectivities of the 15 auditory cortical regions from contralateral cortical areas are shown in Supplementary Fig. S2, and to contralateral cortical regions in Supplementary Fig. S3.

A feature of the effective connectivities is that they are strongest to the corresponding brain region contralaterally. This is shown for example by the diagonal line of high effective connectivities in Supplementary Figs. S2 and S3 running from region 52 to region STSvp (and noting that this is the case also for TA2). This attests to the power of the effective connectivity algorithm, for it detects corresponding particular brain regions in the contralateral hemisphere. Also, this is an interesting principle of brain connectivity, which implies that the contralateral connectivities provide especially for comparison and support between regions performing similar processing in the other hemisphere, rather than providing for hierarchical computations between the two hemispheres.

The contralateral effective connectivities are in general weaker than those ipsilaterally. The ratio across the matrices shown in Fig. 2 and Supplementary Fig. S2 was that the contralateral effective connectivities were 63% of the ipsilateral effective connectivities.

Downloaded from https://academic.oup.com/cercor/article/33/10/6207/6960609 by University of Warwick user on 15 May 2023

It is notable that the left STS cortical regions have much less effective connectivity with non-STS contralateral cortical regions than with ipsilateral non-STS cortical regions (Supplementary Figs. S2 and S3). This is consistent with the evidence considered in the section Discussion that these STS regions are quite lateralized and are involved in semantic representations and language processing.

Differences of effective connectivities of the right vs left hemisphere for the 15 auditory cortical regions

Most of the analyses presented so far have been for the left hemisphere, or of the left hemisphere with the right hemisphere. For completeness, the differences of effective connectivity for the right *minus* the left hemisphere for the 15 auditory cortical regions are shown in Supplementary Figs. S6 and S7. In addition, Supplementary Fig. S8 shows the effective connectivity for the right hemisphere from cortical regions to the auditory regions for comparison with Fig. 2 and Supplementary Fig. S9 shows the effective connectivity for the right hemisphere to cortical regions from the auditory regions for comparison with Fig. 3. One implication of what is shown in Supplementary Figs. S6 and S7 is that the connectivities of most of the auditory cortical regions 52 to TA2 in these figures) are stronger in the right than the left hemisphere. This is consistent with concepts that auditory and perhaps especially auditory-spatial processing is somewhat more a feature of the right than the left hemisphere (Spierer et al. 2009). For the STS cortex regions, the reverse is the case, and the connectivities in the left hemisphere are generally stronger, consistent with their connectivity with language regions of the cortex in the left hemisphere. Furthermore, comparison of Fig. 3 with S9 shows that in the left hemisphere the STS regions (STGa, STSda, STSdp, STSva, STSvp) have more and stronger effective connectivity directed towards Broca's area regions 45, and 44, and the closely associated 47 l, and towards 55b the premotor language-related region. Conversely, the STS regions on the right may have stronger connectivity to the (right) hippocampus. In addition, on the left, the first set of auditory cortical regions (52 to RI) may have stronger connectivity to language-related areas superior temporal visual (STV) and TPOJ1 regions (Supplementary Fig. S9). Comparing Supplementary Fig. S2 with Supplementary Fig. S8 suggests more effective connectivity from the fusiform face area FFC (implicated in face, object and word form processing) to the STS regions in the right hemisphere.

Functional connectivity and diffusion tractography

The functional connectivity is shown in Fig. 5, and the diffusion tractography in Fig. 6 for comparison with the effective connectivity. Functional connectivity and diffusion tractography have been used in many previous investigations of the human connectome (Catani and Thiebaut de Schotten 2008; Glasser et al. 2016a; Maier-Hein et al. 2017), and therefore the comparison with effective connectivity is of interest.

The functional connectivities (Fig. 5), which represent a linear measure of connectivity (calculated with the Pearson correlation) range from close to 1.0 to −0.33 and with a threshold of 0.4 reveal somewhat more links than the effective connectivity, partly perhaps because they can reflect common input to two regions rather than causal connectivity between regions, and partly because the threshold has been set to reveal effects known in the literature but not reflected in the effective connectivity. The functional connectivities are useful as a check on the effective connectivities, but of course do not measure causal effects. One difference of the functional connectivity is that (at this threshold) it does not show connectivity between FFC and STS regions (Fig. 5), whereas this is revealed by the effective connectivity (Fig. 2). Another difference is that the functional connectivity is rather non-discriminative between the somatosensory regions with connectivity with auditory cortical regions (Fig. 5), whereas the effective connectivity is much more selective in showing which somatosensory regions influence which auditory cortex regions (Fig. 2). The functional connectivity in the right hemisphere (Supplementary Fig. S10) has differences from those in the left hemisphere (Fig. 5) that are consistent with the differences in effective connectivity described above.

The diffusion tractography (Fig. 6) again provides no evidence on the direction or causality of connections, and is useful as it can provide some evidence on what in the effective connectivity may reflect a direct connection, and what does not. However, limitations of the diffusion tractography are that it cannot follow streamlines within the gray matter so the exact site of termination is not perfectly provided; and the tractography does not follow long connections well with for example almost none of the contralateral connectivity shown with tractography that is revealed by the effective connectivity in Supplementary Figs. S2 and S3; and may thus overemphasize connections between close cortical regions. Nevertheless the diffusion tractography is a useful complement to the effective connectivity, especially where it provides evidence where an effective connectivity link may be mediated by a direct connection. On the other hand, the effective connectivity and functional connectivity are useful complements to the tractography by helping to exclude false positives in the tract-following in the tractography, as had been examined for the human hippocampal connectome (Huang et al. 2021; Ma et al. 2022; Rolls et al. 2022f). The diffusion tractography (Fig. 6) does not show many connections between auditory cortex regions and visual cortex before the temporal lobe or somatosensory regions apart from FOP1-OP2-3, so these effective connectivities (Fig. 2) may be indirect, or may be missed by the tractography because they are relatively long range. The connections of inferior parietal regions such as PF, PFm, and PGs with auditory cortical regions is more evident with the tractography (Fig. 6) than with the effective connectivity. The connections of a number of auditory cortical regions with Broca's area 44 (which is the endpoint of the auditory dorsal stream (ADS) (Rauschecker and Scott 2009) and is implicated in syntax (Friederici et al. 2017)) is especially evident with the diffusion tractography. The diffusion tractography is thus a useful complement to the resting state effective connectivity, and provides an indication of what might be revealed by the effective connectivity in language-related tasks.

Correlations between the connectivities of different cortical regions

A comparison of Supplementary Fig. S4 with Supplementary Fig. S5, which shows the correlations between the functional connectivities of the 15 auditory cortical regions, indicates that the effective connectivity is much more selective than functional connectivity in revealing the different connectivities of different cortical regions, and which regions have similar connectivity. Supplementary Fig. S4 shows for example that the STS regions have effective connectivities that are similar to each other, but also with A5 (which latter has effective connectivities to STS regions). In addition, RI is shown to have effective connectivity that is similar primarily to area 52 (Supplementary Fig. S4).

Downloaded from https://academic.oup.com/cercor/article/33/10/6207/6960609 by University of Warwick user on 15 May 2023

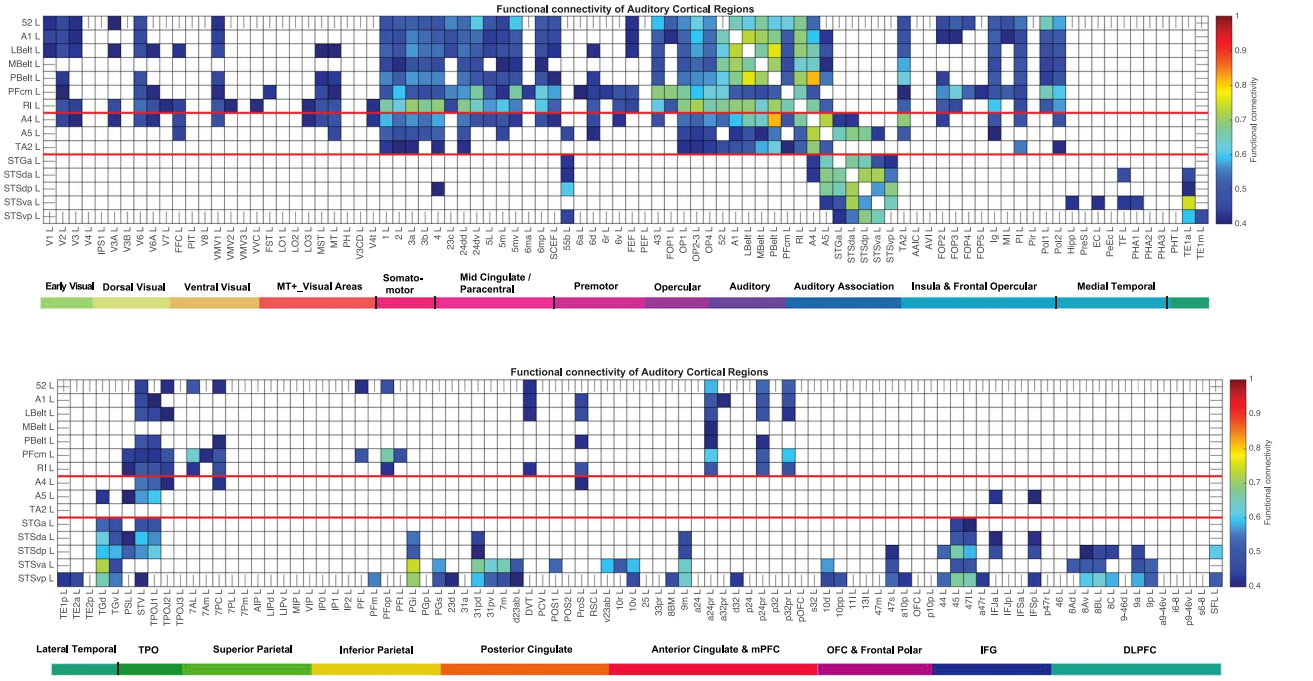

Fig. 5. Functional connectivity between auditory cortical regions and 180 other cortical regions in the left hemisphere. Functional connectivities less than 0.4 are shown as blank. The upper figure shows the functional connectivity of the auditory cortical regions with the first half of the cortical regions; the lower figure shows the functional connectivity with the second half of the cortical regions. The color scale shows the value of the functional connectivity from the threshold used here of 0.4 to a maximum possible value of 1.0. Abbreviations: See Supplementary Table S1. Conventions as in Fig. 2.

These points are less clear from the functional connectivity (Supplementary Fig. S5).

Discussion

A schematic overview of the effective connectivity of the auditory cortical system is shown in Fig. 7 and b. A simplified schematic organization is that regions A1 and 52 > LBelt and MBelt > PBelt > A4 (Here > indicates "has effective connectivity to," though some connectivity may cross levels of the hierarchy.) That part of the connectivity appears to be hierarchical, taking into account the evidence shown in Fig. 3. After A4 there may be a split in the pathways in humans, given the evidence in Figs. 3 and 2. In one stream, A4 has effective connectivity to TA2, and TA2 given its location is likely to be a ventral stream region. TA2 has interesting connectivity to the parainsular region PI. In a second stream, A4 has EC to A5, which then connects to dorsal bank superior temporal sulcus (STS) regions STGa, STSda, and STSdp, which then have onward effective connectivity to TPOJ1, STV, PSL, TGv, TGd, and PGi (Fig. 3), which are language-related regions as defined and investigated elsewhere (Rolls et al. 2022e). A5 is higher in the hierarchy than A4, in that A4 receives from A1 and 52, and A5 from PBelt, LBelt, and A4 (Figs. 2 and 3).

In the following Discussion, the strengths of the effective connectivities are used as a guide; but also is the point made earlier that effective connectivity in the backward direction in a cortical hierarchical system does not reflect the transfer of the properties represented at a higher level but instead the capability for top-down attention and for memory recall. Other guides are findings from neuronal recordings in comparable regions in macaques and activations in humans.

Functional implications and cortical streams

The effective connectivity in humans described here provides evidence for hierarchical processing from core regions (A1 and 52), through the LBelt/MBelt and then PBelt regions, to A4. A4 is an extended region in the anterior–posterior direction, and future studies might show that it can be subdivided.

In one stream after A4, A4 has effective connectivity to TA2, and TA2, given its location, is likely to be a ventral stream region. TA2 has some effective connectivity to STGa; and to MT, MST, V6, V3A, etc.; and with region 1 (somatosensory). However, STGa cannot be regarded as a region that mainly receives from TA2, for as described in the Results the connectivity to STGa from A5 is ten times stronger than that from TA2. TA2 also has interesting connectivity from the parainsular region PI. PI has auditory and visual as well as somatosensory inputs (Rolls et al. 2022a) (Rolls et al. 2022e), rendering it a region for multisensory convergence.

In another stream, A4 has effective connectivity to A5, which then connects to (anatomically dorsal) superior bank temporal sulcus (STS) regions STGa, STSda, and STSdp, which then have onward effective connectivity to TPOJ1, STV, PSL, TGv, TGd, and PGi (Fig. 3), which are language-related regions (Rolls et al. 2022e). The dorsal bank STS regions (STSda and STSdp) also receive visual inputs about, for example, the movements made by the face and mouth during speaking, in that some neurons in these cortical regions of macaques respond perfectly to the small lip and mouth movements made by humans when they speak (Hasselmo et al. 1989a, 1989b). We discovered neurons in the same cortical regions that respond to auditory stimuli including vocalization (Baylis et al. 1987), and indeed some neurons in this cortical region respond to both visual and auditory stimuli (Khandhadia et al. 2021). The functions of these STS regions and their onward connectivity are considered next.

Downloaded from https://academic.oup.com/cercor/article/33/10/6207/6960609 by University of Warwick user on 15 May 2023

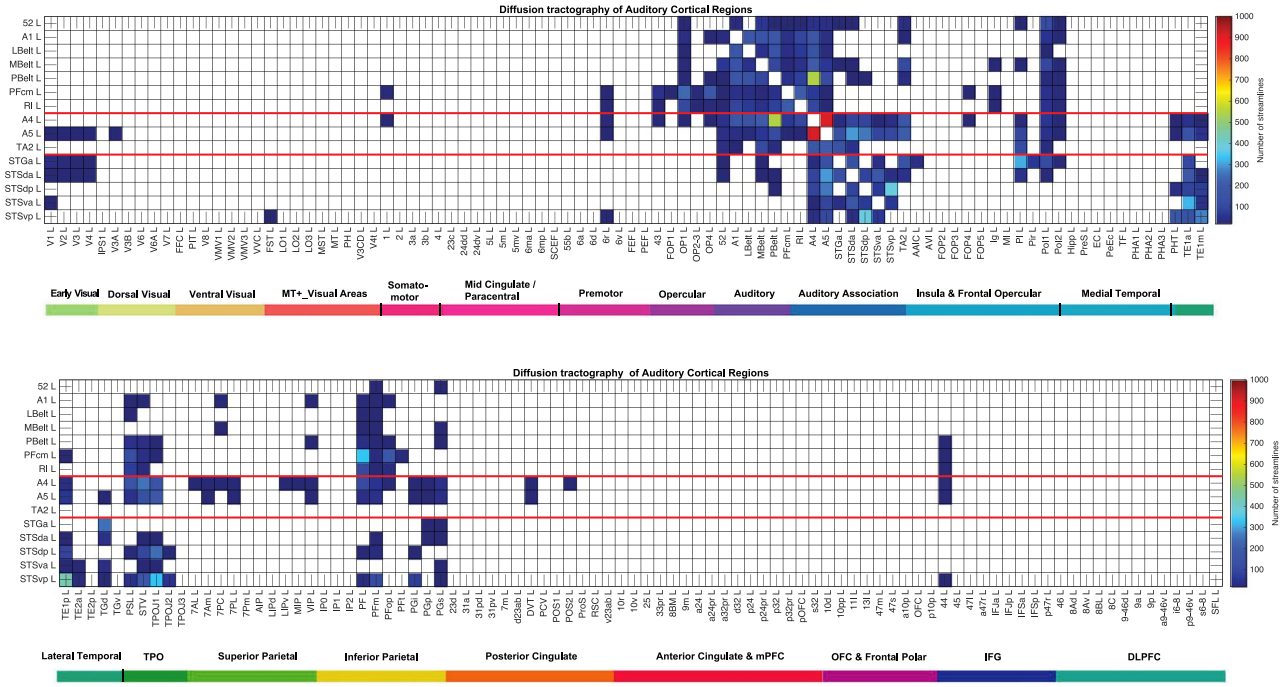

Fig. 6. Connections between the auditory cortical regions and 180 other cortical regions in the left hemisphere as shown by diffusion tractography using the same layout as in Figs. 2 and 5. The number of streamlines shown was thresholded at 10 and values less than this are shown as blank. The color bar maximum was set to 1000 streamlines to show some detail for the lower values, and the maximum number of streamlines across the brain regions shown was 1100 (excluding a few outliers). Abbreviations: See Supplementary Table S1. Conventions as in Fig. 2.

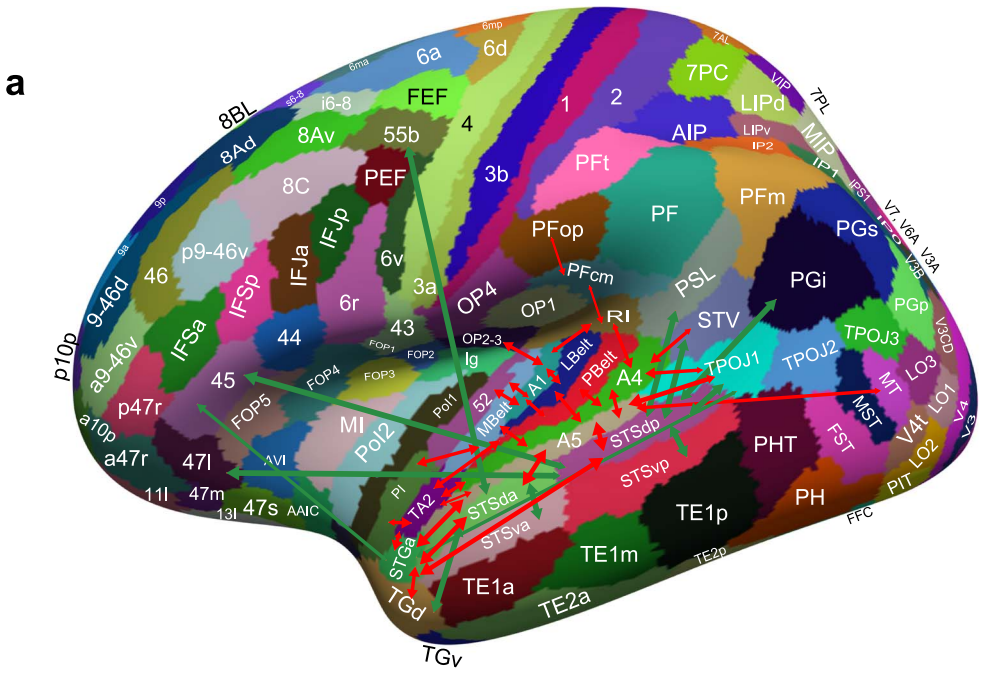

Auditory system: lateral view

Fig. 7a. Effective connectivity of human auditory cortical regions shown schematically. The widths of the lines and the size of the arrowheads indicate the magnitude and direction of the effective connectivity. The red arrows show the main auditory HCP-MMP division connectivity (regions 52 to TA2), and the green arrows further connectivity (involving STS regions). A simplified schematic organization is that region A1 > LBelt, MBelt and 52 > PBelt > A4 > A5 > STGa, STSda, STSdp > TPOJ1, STV, PGi (Here > indicates has effective connectivity to, though some connectivity may cross levels of the hierarchy.) somatosensory cortical regions have connectivity with A1, RI, TA2, etc. MT has connectivity to A5. TPOJ1, STV, PSL, STSdp and STSda are involved in language as analyzed elsewhere (Rolls et al. 2022e). Connections between early cortical auditory regions and area 44 in what may be a dorsal language related auditory stream are described in the text. Lbelt, Pbelt, A4 and A5 have effective connectivity with MT/MST regions as indicated, and this may be part of a dorsal "where" stream leading to intraparietal and area 7 regions (see text).

Downloaded from https://academic.oup.com/cercor/article/33/10/6207/6960609 by University of Warwick user on 15 May 2023

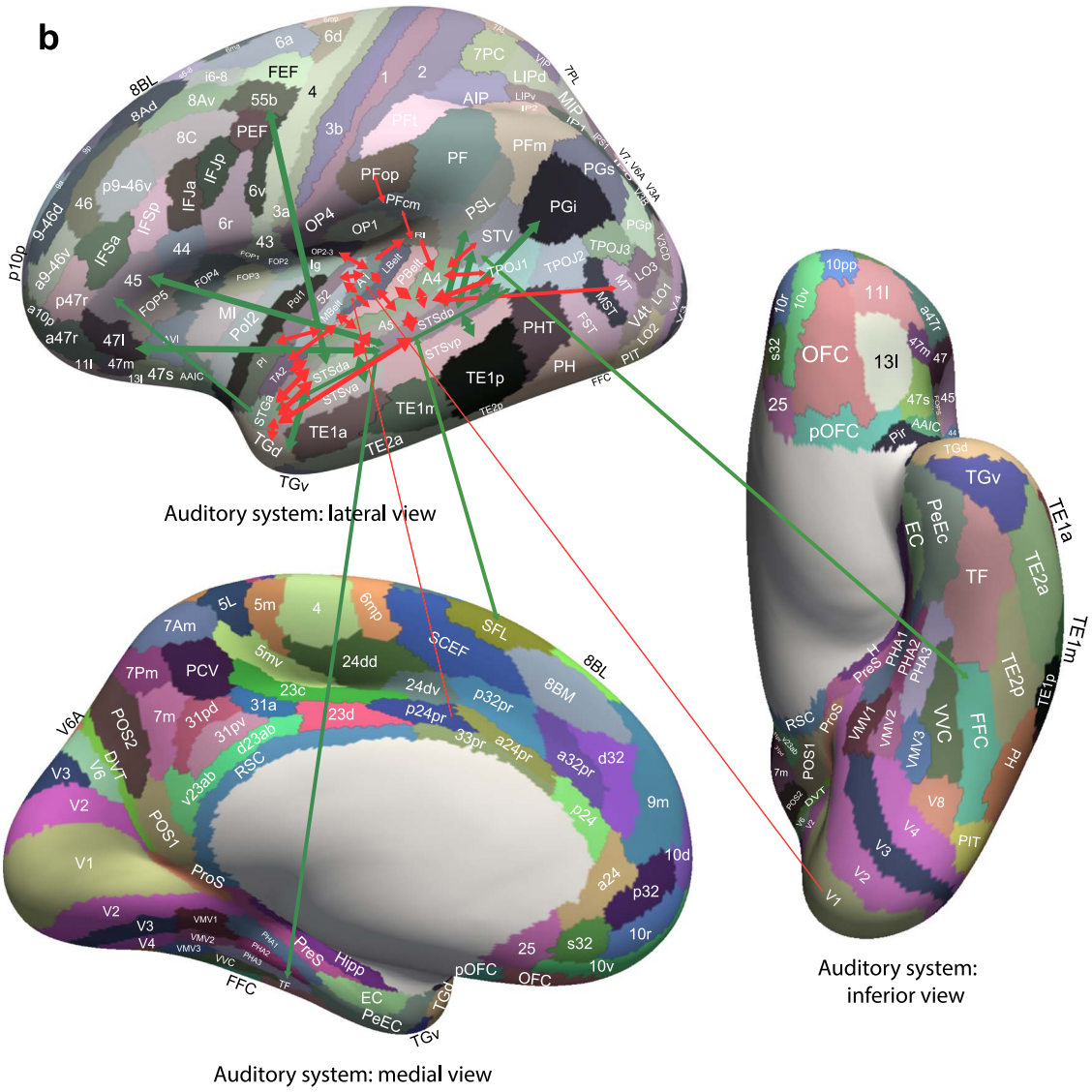

Fig. 7b. Effective connectivity of the auditory cortical regions with other cortical regions. The widths of the lines and the size of the arrowheads indicate the magnitude and direction of the effective connectivity. The red arrows show the main auditory HCP-MMP division connectivity (regions 52 to TA2), and the green arrows further connectivity (involving STS regions). Conventions as in Fig. 7a.

Dorsal vs ventral auditory processing streams in humans

Evidence for dorsal and ventral auditory streams in macaques, with some consistent evidence in humans, was described in the section Introduction (Rauschecker and Scott 2009; Rauschecker 2018a). A summary was that in humans a ventral auditory stream involves anterior auditory temporal cortical regions that connect via the anterior part of the temporal lobe to the inferior frontal gyrus including especially area 45 (Rauschecker 2012). A dorsal auditory stream was described as involving the posterior auditory cortical regions connecting via inferior parietal regions to premotor cortex 6, region 44, etc. (Rauschecker 2012).

A4 does connect strongly to TA2 in the anterior temporal lobe, and that could indeed be part of a ventral auditory stream. But A4 also projects to A5, and the issue arises of whether A5 is part of a dorsal or ventral auditory stream. In practice, A5 has connectivity to dorsal bank temporal sulcus (STS) regions STGa, STSda, and STSdp, which then have onward effective connectivity to TPOJ1, STV, PSL, TGv, TGd, and PGi (Fig. 3). These latter regions are considered language-related and have connectivity directed to Broca's area, and especially to 45 compared to 44 (Rolls et al. 2022e). The dorsal bank STS regions (STSda and STSdp) also receive visual inputs about, for example, the movements made by the face and mouth during speaking (Baylis et al. 1987; Hasselmo et al. 1989a, 1989b), and may combine these (Belin 2019; Khandhadia et al. 2021), which makes them important for the decoding of articulator movements. These dorsal bank STS regions are therefore important in linking motion-related changes in the sight of the face to the dynamically changing auditory input, and this is likely to be useful for identifying who in a group is making the vocalization, in maximizing the ability to decode information in noisy environments in order to understand speech, in maximizing the information in social signals by combining the auditory and visual components, etc. In the sense that this processing provides evidence about what the message is, this could be considered as a type of ventral stream "what" semantic processing.

That leads us to consider the dorsal "how" stream for auditory processing related to language (Rauschecker and Scott 2009; Rauschecker 2018a). In the present analysis, the diffusion

Downloaded from https://academic.oup.com/cercor/article/33/10/6207/6960609 by University of Warwick user on 15 May 2023

tractography does show connections of PBelt, RI, A4 and A5 with Broca's area 44 (Fig. 6), and this may be how the dorsal "how" language-related stream is reflected in the present analysis. Corresponding effective or functional connectivity was not identified in the present analysis, perhaps because it is functionally relatively weak, or perhaps because the data were acquired in the resting state not during language production.

Perhaps in auditory processing, evidence about the spatial location of sounds, inter alia to facilitate spatial attention including by moving the eyes and by top-down attentional space-based modulation, could be considered another dorsal stream type of function, and that is likely to be implemented in parts of dorsal brain regions such as those in the intraparietal sulcus and area 7. Indeed A4 and A5, and some earlier cortical regions, do have effective connectivity to regions including MT and MST (Fig. 3), which in turn have effective connectivity to intraparietal and thereby parietal area 7 regions (Rolls et al. 2022b), and this connectivity might be considered as part of a dorsal auditory stream. This analysis is supported by the functional connectivity, which is evident in Fig. 5 between A4, the PBelt, etc. and parietal 7AL, 7Am, and 7PC, and is also supported by the diffusion tractography showing connections between similar regions (Fig. 6). These auditory inputs to dorsal-stream parietal areas could be used to shift visual attention and eye position to a source of sound, to help track moving noisy objects such as flying birds and predators (e.g. alarm calls for eagles versus snakes (Seyfarth and Cheney 2010)), or keeping track of the location of a predator when running away, and performing actions in the dark for objects that can be detected by their sound.

In terms of Broca's area, 45 has more effective connectivity than 44 with STGa, STSda and STSdp and related regions such as TGv (Figs. 2 and 3 and Rolls et al. (2022e)), which are anterior temporal lobe semantic regions (Rolls et al. 2022e). The diffusion tractography shows more connections of 44 than 45 with PBelt, A4, A5, and STSvp (Fig. 6), and with premotor area 6 regions (Rolls et al. 2022e). In addition to the hypotheses that region 45 which is anterior in the frontal lobes is connected with anterior temporal lobe semantic systems (e.g. in the dorsal bank of the STS), and that region 44 more posteriorly in the frontal lobes is more connected with more posterior temporal lobe auditory regions involved in "how" processing, it is further proposed that there is information flow from 45 to 44 as part of a route from semantic to language output in terms of speech production and articulation (Rauschecker and Scott 2009; Rauschecker 2018a; Rolls et al. 2022e).

One point to note is that A4 and A5 are long regions that are likely in future to be subdivided into anterior and posterior parts. Similarly, at earlier stages of auditory processing, single-unit studies on macaques (Rauschecker et al. 1995) have shown that LBelt and PBelt can already be subdivided into subregions with mirror-symmetric target regions, a major shortcoming of the original HCP.

Cortex in the dorsal bank of the superior temporal sulcus: a system for multimodal semantic representations including visual motion, auditory, and somatosensory information

Visual inputs reach STSdp from PGi, and provide a route for moving visual stimuli/objects analyzed in the parietal cortex to reach STS regions (Rolls et al. 2022b, 2022d). Visual inputs also reach STSdp from the Superior Temporal Visual (STV) region, which receives from both MT and FFC (Rolls et al. 2022b, 2022e), and which could contribute to the neuronal activity in the cortex in the STS, which has been shown to respond to moving heads, faces, and objects in macaques (Hasselmo et al. 1989a; Hasselmo et al. 1989b; Khandhadia et al. 2021), and which is identified as a third visual stream involved in processing socially relevant stimuli (Baylis et al. 1987; Rolls 2014; Pitcher and Ungerleider 2021; Rolls 2021c; Rolls et al. 2022b). STSda and STSdp also have connectivity from STSva and STSvp, which have strong connectivity with the Ventrolateral Visual "What" Stream (Rolls et al. 2022b). STSda and STSdp also receive auditory effective connectivity from A5, and neurons in macaque face patch AF in the STS can be influenced by auditory as well as by visual stimuli (Khandhadia et al. 2021). STSdp has connectivity directed towards Broca's area especially 45 and the closely related 47 l and less to 44, and to the PeriSylvian Language region PSL and to the Superior Frontal Language region SFL (Rolls et al. 2022e).

This "superior/dorsal bank STS cortex system" thus enables multimodal representations including visual, auditory, and probably also somatosensory via PGi, to gain access to the language system (Rolls et al. 2022e). This is a major output of cortical visual and auditory processing for use in language, described in more detail elsewhere (Rolls et al. 2022e). Indeed, this dorsal bank STS semantic stream has stronger connectivity to 45 than to 44, consistent with the hypothesis that this is part of a ventral auditory "what" stream (Rauschecker and Scott 2009; Rauschecker 2018a). There is also a link from this system via TF to the hippocampal memory system (Rolls et al. 2022b).

Discoveries in macaques provide an indication for what is represented in these STS regions. It was discovered that single neurons in the macaque STS respond to face expression and also to face and head movement to encode the social relevance of stimuli (Hasselmo et al. 1989a, 1989b). For example, a neuron might respond to closing of the eyes, or to turning of the head away from facing the viewer, both of which break social contact (Hasselmo et al. 1989a, 1989b). Some neurons respond to the direction of gaze (Perrett et al. 1987). It was found that many of the neurons in the STS respond only or much better to moving faces or objects (Hasselmo et al. 1989a), whereas in the anterior inferior temporal cortex, neurons were discovered that respond well to static visual stimuli, and are tuned for face identity (Perrett et al. 1979; Perrett et al. 1982; Desimone et al. 1984; Rolls 1984; Hasselmo et al. 1989a; Rolls et al. 1997a, 1997b; Rolls 2000; Rolls and Treves 2011; Chang and Tsao 2017). It has been proposed that PGi, with its inputs from PGs, which has connectivity with superior parietal and intraparietal regions that encode visual motion, is part of this processing stream for socially relevant face-related information (Rolls et al. 2022d). Consistent with this, the effective connectivity is stronger from PGi to STS regions (Figs. 2-4). In humans, representations of this type could provide part of the basis for the development of systems to interpret the significance of such stimuli, including theory of mind. Consistent with this proposal, activations in the temporo-parietal junction (TPJ) region are related to theory of mind (Schurz et al. 2017; Buckner and DiNicola 2019; DiNicola et al. 2020). Signals of this type are important in understanding the meaning of seen faces and objects, and indeed evidence about moving objects present in the STS may reach it from PGs and PGi, which in turn receive connectivity from the intraparietal sulcus regions (Rolls et al. 2022d) in which neurons respond to visual motion and to grasping objects, which are important in tool use (Maravita and Romano 2018), which is another fundamental aspect of the meaning or semantics of stimuli. We proposed that the cortex in the STS in which neurons respond to moving faces, eyes, etc. and to changing facial

Downloaded from https://academic.oup.com/cercor/article/33/10/6207/6960609 by University of Warwick user on 15 May 2023

expression enables ventral stream "what" information to be combined with dorsal stream visual motion information to form a third visual stream, and that this could be useful for social functions (Hasselmo et al. 1989a, 1989b), especially as this system projects to the orbitofrontal cortex/vmPFC where similar types of neuronal response are found (Rolls et al. 2006). The concept that this STS cortical system is important in social behavior has recently gained support (Pitcher et al. 2019; Pitcher and Ungerleider 2021). Moreover, neurons can respond to auditory stimuli such as vocalization both in the STS regions (Baylis et al. 1987) and in the orbitofrontal cortex, which receives connections from the STS (Rolls et al. 2006). The connectivity described here helps to provide a functional framework for the processing streams involved in these types of function.

Other auditory system cortical connectivities

Another feature of the auditory cortical connectivity described here is the connectivity with somatosensory cortical areas, with, for example, connectivity from somatosensory cortical area 1 to auditory cortical regions A4 and A5; and the earlier auditory cortex regions have connectivity with the supracallosal anterior cingulate regions a24pr, a32pr, p24pr, and p32pr, which have somatosensory/motor connectivity (Rolls et al. 2022h) (Figs. 2-4). This might relate to directing auditory attention to any touch to the body; to behaviors that might be performed before a highly developed visual system evolved; and to navigation/obstacle avoidance in the dark. Another type of somatosensory feedback may be needed in speech production, especially during early learning of articulation, where it may be crucial for the distinction between different types of consonants (Ohashi and Ostry 2021).

In addition, there is evidence for effective connectivity of some auditory cortical regions to the hippocampus, and to the scene-related VMV1 (Sulpizio et al. 2020), with both types of connectivity involved in episodic memory (Rolls et al. 2022a, 2022b, 2022f) (Figs. 2-4).

In addition, auditory cortical region A5 has connectivity with inferior frontal gyrus regions IFJa and IFSp, which are implicated in short-term working memory for the ventral streams (Plakke and Romanski 2014; Miller et al. 2018; Passingham 2021; Rolls et al. 2022a).

The auditory cortex connectivity with inferior parietal regions is primarily between the STS visual–auditory regions and PGi, with some connectivity also with PGs and PFm (Figs. 2-4), all of which are visual inferior parietal regions linked considerably to ventral stream processing (Rolls et al. 2022d, 2022e).

Inputs related to reward and punishment from, for example, the ventromedial prefrontal cortex (vmPFC) (10r, 10v, 10d), and orbitofrontal cortex (a47r) (Rolls et al. 2022g) reach STS auditory–visual cortical regions where objects, faces, and their semantic meaning are represented (Rolls et al. 2022e), rather than earlier stages of auditory cortical processing (Figs. 2-4). Correspondingly, STS regions have effective connectivity with some orbitofrontal/vmPFC regions in which neurons respond to vocalization and the face movements that produce them (Rolls et al. 2006).

Conclusions

The effective connectivity, complemented by functional connectivity and diffusion tractography, provides evidence consistent with a hierarchy of auditory cortical processing in humans similar to nonhuman primates (Pandya 1995; Kaas and Hackett 2000) from a Core region (A1), to Belt regions LBelt and MBelt, and transitional region 52, which may be a belt region (Brodmann 1909); then to PBelt; and then to higher regions (A4 and A5). A4 has connectivity to TA2 in the anterior temporal lobe, which makes it part of a ventral auditory stream implicated in semantic object processing (Rauschecker and Tian 2000; Rauschecker and Scott 2009). A4 also has effective connectivity to A5, which then connects to dorsal bank superior temporal sulcus (STS) regions STGa, STSda, and STSdp. These STS regions also receive visual inputs about moving faces and objects, and the auditory and visual streams are combined to help in multimodal object identification, such as who is speaking, what is being said, what the object is, etc. This system can thus also be considered as an important part of the ventral auditory "what" stream. Consistent with the dorsal bank STS regions being part of a ventral auditory stream, the dorsal bank STS regions then have effective connectivity to TPOJ1, STV, PSL, TGv, TGd, and PGi (Fig. 3), which are language-related regions involved in semantic representations about objects, faces, etc. using multimodal information, and which then connect to Broca's area, especially to area 45 (Rolls et al. 2022e). Diffusion tractography indicated connections of PBelt, RI, A4, and A5 with Broca's area 44 (Fig. 6), and this may be how the dorsal "how" language stream (Rauschecker and Scott 2009; Rauschecker 2018a) is reflected in the present analysis. Corresponding effective or functional connectivity was not identified in the present analysis, perhaps because it is functionally relatively weak, or perhaps because the data were acquired in the resting state. In the monkey, there is a rostral and a caudal parabelt (Kaas and Hackett 2000), and that distinction is not made in the HCP-MMP (Glasser et al. 2016a), but if such a separation can be made in humans, that might provide further evidence about dorsal and ventral language-related streams. A4 and A5, and some earlier cortical regions, have in addition effective connectivity to regions including MT and MST (Fig. 3), which in turn have effective connectivity to intraparietal and thereby parietal area 7 regions (Rolls et al. 2022b). This connectivity might be considered as part of a dorsal auditory "where" stream (Rauschecker and Tian 2000; Rauschecker 2018a) involved in actions in space that utilize auditory information.

Supplementary material

Supplementary material is available at *Cerebral Cortex* online.

Data and code availability

The data are available at the HCP website http://www.humanconnectome.org/. Code for the Hopf effective connectivity algorithm is available at https://github.com/decolab/Effective-Connectivity--Hopf.

Author contributions

Edmund Rolls designed and performed the research, and wrote the paper, did conceptualization, data curation, formal analysis, investigation, methodology, project administration, resources, software, supervision, validation, visualization, writing—original draft, writing—review & editing. Josef Rauschecker: Conceptualization, Interpretation; Writing—review & editing. Gustavo Deco provided the effective connectivity algorithm and methodology, resources, software, writing—review & editing. Chu-Chung Huang performed the diffusion tractography and prepared the brain figures with the HCP-MMP labels and did data curation, investigation, methodology, visualization, writing—review & editing.

Downloaded from https://academic.oup.com/cercor/article/33/10/6207/6960609 by University of Warwick user on 15 May 2023

Jianfeng Feng performed the funding acquisition, project administration, writing—review & editing. All authors approved the paper.

Acknowledgements

The neuroimaging data were provided by the Human Connectome Project, WU-Minn Consortium (Principal Investigators: David Van Essen and Kamil Ugurbil; 1U54MH091657) funded by the 16 NIH Institutes and Centers that support the NIH Blueprint for Neuroscience Research; and by the McDonnell Center for Systems Neuroscience at Washington University. Dr Wei Cheng and Shitong Xiang of ISTBI, Fudan University, Shanghai are thanked for parcellating the data into HCP-MMP surface-based space (Glasser et al. 2016a) and reordering it into HCPex order (Huang et al. 2022). Roscoe Hunter of the University of Warwick is thanked for contributing to the description in the Supplementary Material of the Hopf effective connectivity algorithm.

Conflict of interest statement: The authors have no competing interests to declare.

Funding

The work was supported by the following grants. Professor J. Feng: National Key R&D Program of China (No. 2019YFA0709502); 111 Project (No. B18015); Shanghai Municipal Science and Technology Major Project (No. 2018SHZDZX01), ZJLab, and Shanghai Center for Brain Science and Brain-Inspired Technology; and National Key R&D Program of China (No. 2018YFC1312904). G.D. is supported by a Spanish national research project (ref. PID2019-105772GB-I00 MCIU AEI) funded by the Spanish Ministry of Science, Innovation and Universities (MCIU), State Research Agency (AEI); HBP SGA3 Human Brain Project Specific Grant Agreement 3 (grant agreement no. 945539), funded by the EU H2020 FET Flagship programme; SGR Research Support Group support (ref. 2017 SGR 1545), funded by the Catalan Agency for Management of University and Research Grants (AGAUR); Neurotwin Digital twins for model-driven non-invasive electrical brain stimulation (grant agreement ID: 101017716) funded by the EU H2020 FET Proactive programme; euSNN European School of Network Neuroscience (grant agreement ID: 860563) funded by the EU H2020 MSCA-ITN Innovative Training Networks; CECH The Emerging Human Brain Cluster (Id. 001-P-001682) within the framework of the European Research Development Fund Operational Program of Catalonia 2014–2020; Brain-Connects: Brain Connectivity during Stroke Recovery and Rehabilitation (id. 201725.33) funded by the Fundacio La Marato TV3; Corticity, FLAG¨ERA JTC 2017 (ref. PCI2018–092891) funded by the Spanish Ministry of Science, Innovation and Universities (MCIU), State Research Agency (AEI). This work was also supported by NSF-BCS-0519127, NSF-OISE-0730255, NIDCD-1RC1DC010720, and NIDCD-1R01DC014989 grants (to J.P.R.). The funding sources had no role in the study design; in the collection, analysis, and interpretation of data; in the writing of the report; and in the decision to submit the article for publication.

Ethical permissions

No data were collected as part of the research described here. The data were from the Human Connectome Project, and the WU-Minn HCP Consortium obtained full informed consent from all participants, and research procedures and ethical guidelines were followed in accordance with the Institutional Review Boards (IRB), with details at the HCP website http://www.humanconnectome.org/

References

Ahveninen J, Huang S, Nummenmaa A, Belliveau JW, Hung AY, Jaaskelainen IP, Rauschecker JP, Rossi S, Tiitinen H, Raij T. Evidence for distinct human auditory cortex regions for sound location versus identity processing. *Nat Commun*. 2013:4:2585.

Amunts K, Zilles K. Architecture and organizational principles of Broca's region. *Trends Cogn Sci*. 2012:16:418–426.

Amunts K, Lenzen M, Friederici AD, Schleicher A, Morosan P, Palomero-Gallagher N, Zilles K. Broca's region: novel organizational principles and multiple receptor mapping. *PLoS Biol*. 2010:8:9.

Archakov D, DeWitt I, Kusmierek P, Ortiz-Rios M, Cameron D, Cui D, Morin EL, VanMeter JW, Sams M, Jaaskelainen IP et al. Auditory representation of learned sound sequences in motor regions of the macaque brain. *Proc Natl Acad Sci U S A*. 2020:117:15242–15252.

Bajaj S, Adhikari BM, Friston KJ, Dhamala M. Bridging the gap: dynamic causal Modeling and Granger causality analysis of resting state functional magnetic resonance imaging. *Brain Connect*. 2016:6:652–661.

Baker CM, Burks JD, Briggs RG, Conner AK, Glenn CA, Taylor KN, Sali G, McCoy TM, Battiste JD, O'Donoghue DL et al. A Connectomic atlas of the human cerebrum-chapter 7: the lateral parietal lobe. *Oper Neurosurg (Hagerstown)*. 2018a:15:S295–S349.

Baker CM, Burks JD, Briggs RG, Milton CK, Conner AK, Glenn CA, Sali G, McCoy TM, Battiste JD, O'Donoghue DL et al. A Connectomic atlas of the human cerebrum-chapter 6: the temporal lobe. *Oper Neurosurg (Hagerstown)*. 2018b:15:S245–S294.

Balezeau F, Wilson B, Gallardo G, Dick F, Hopkins W, Anwander A, Friederici AD, Griffiths TD, Petkov CI. Primate auditory prototype in the evolution of the arcuate fasciculus. *Nat Neurosci*. 2020:23:611–614.

Baylis GC, Rolls ET, Leonard CM. Functional subdivisions of the temporal lobe neocortex. *J Neurosci*. 1987:7:330–342.

Belin P. The vocal brain: Core and extended cerebral networks for voice processing. In: Belin P, editors. *Fruhholz S*. Oxford Handbook of Voice Perception Oxford: Oxford University Press p; 2019. pp. 37–60

Belin P, Zatorre RJ. 'What', 'where' and 'how' in auditory cortex. *Nat Neurosci*. 2000:3:965–966.

Bornkessel-Schlesewsky I, Schlesewsky M, Small SL, Rauschecker JP. Neurobiological roots of language in primate audition: common computational properties. *Trends Cogn Sci*. 2015a:19:142–150.

Bornkessel-Schlesewsky I, Schlesewsky M, Small SL, Rauschecker JP. Response to Skeide and Friederici: the myth of the uniquely human 'direct' dorsal pathway. *Trends Cogn Sci*. 2015b:19:484–485.

Brodmann K. *Vergleichende Lokalisationslehre der Grosshirnrinde in ihren Prinzipien dargestellt auf Grund des Zellenbaues*. Leipzig: Barth; 1909

Buckner RL, DiNicola LM. The brain's default network: updated anatomy, physiology and evolving insights. *Nat Rev Neurosci*. 2019:20:593–608.

Catani M, Thiebaut de Schotten M. A diffusion tensor imaging tractography atlas for virtual in vivo dissections. *Cortex*. 2008:44:1105–1132.

Chang L, Tsao DY. The code for facial identity in the primate brain. *Cell*. 2017:169:1013–1028.e1014.

Colclough GL, Smith SM, Nichols TE, Winkler AM, Sotiropoulos SN, Glasser MF, Van Essen DC, Woolrich MW. The heritability of multi-modal connectivity in human brain activity. *elife*. 2017:6:e20178.

Downloaded from https://academic.oup.com/cercor/article/33/10/6207/6960609 by University of Warwick user on 15 May 2023

Corcoles-Parada M, Ubero-Martinez M, Morris RGM, Insausti R, Mishkin M, Munoz-Lopez M. Frontal and insular input to the dorsolateral temporal pole in primates: implications for auditory memory. *Front Neurosci*. 2019:13:1099.

Deco G, Cabral J, Woolrich MW, Stevner ABA, van Hartevelt TJ, Kringelbach ML. Single or multiple frequency generators in on-going brain activity: a mechanistic whole-brain model of empirical MEG data. *NeuroImage*. 2017a:152:538–550.

Deco G, Kringelbach ML, Jirsa VK, Ritter P. The dynamics of resting fluctuations in the brain: metastability and its dynamical cortical core. *Sci Rep*. 2017b:7:3095.

Deco G, Cruzat J, Cabral J, Tagliazucchi E, Laufs H, Logothetis NK, Kringelbach ML. Awakening: predicting external stimulation to force transitions between different brain states. *Proc Natl Acad Sci*. 2019:116:18088–18097.

Desimone R, Albright TD, Gross CG, Bruce C. Stimulus-selective properties of inferior temporal neurons in the macaque. *J Neurosci*. 1984:4:2051–2062.

DeWitt I, Rauschecker JP. Phoneme and word recognition in the auditory ventral stream. *Proc Natl Acad Sci U S A*. 2012:109:E505–E514.

DeWitt I, Rauschecker JP. Wernicke's area revisited: parallel streams and word processing. *Brain Lang*. 2013:127:181–191.

DeWitt I, Rauschecker JP. Convergent evidence for the causal involvement of anterior superior temporal gyrus in auditory single-word comprehension. *Cortex*. 2016:77:164–166.

Dhollander T, Raffelt D, Connelly A. Unsupervised 3-tissue response function estimation from single-shell or multi-shell diffusion MR data without a co-registered T1 image. ISMRM workshop on breaking the barriers of diffusion MRI 5. 2016.

DiNicola LM, Braga RM, Buckner RL. Parallel distributed networks dissociate episodic and social functions within the individual. *J Neurophysiol*. 2020:123:1144–1179.

Erickson LC, Rauschecker JP, Turkeltaub PE. Meta-analytic connectivity modeling of the human superior temporal sulcus. *Brain Struct Funct*. 2017:222:267–285.

Frassle S, Lomakina EI, Razi A, Friston KJ, Buhmann JM, Stephan KE. Regression DCM for fMRI. *NeuroImage*. 2017:155:406–421.

Frey S, Campbell JS, Pike GB, Petrides M. Dissociating the human language pathways with high angular resolution diffusion fiber tractography. *J Neurosci*. 2008:28:11435–11444.

Frey S, Mackey S, Petrides M. Cortico-cortical connections of areas 44 and 45B in the macaque monkey. *Brain Lang*. 2014:131:36–55.

Freyer F, Roberts JA, Becker R, Robinson PA, Ritter P, Breakspear M. Biophysical mechanisms of multistability in resting-state cortical rhythms. *J Neurosci*. 2011:31:6353–6361.

Freyer F, Roberts JA, Ritter P, Breakspear M. A canonical model of multistability and scale-invariance in biological systems. *PLoS Comput Biol*. 2012:8:e1002634.

Friederici AD. Towards a neural basis of auditory sentence processing. *Trends Cogn Sci*. 2002:6:78–84.

Friederici AD, Chomsky N, Berwick RC, Moro A, Bolhuis JJ. Language, mind and brain. *Nat Hum Behav*. 2017:1:713–722.

Friston K. Causal modelling and brain connectivity in functional magnetic resonance imaging. *PLoS Biol*. 2009:7:e33.

Fukushima M, Saunders RC, Leopold DA, Mishkin M, Averbeck BB. Differential coding of conspecific vocalizations in the ventral auditory cortical stream. *J Neurosci*. 2014:34:4665–4676.

Geschwind N. The organization of language and the brain. *Science*. 1970:170:940–944.

Gilson M, Moreno-Bote R, Ponce-Alvarez A, Ritter P, Deco G. Estimation of directed effective connectivity from fMRI functional connectivity hints at asymmetries in the cortical connectome. *PLoS Comput Biol*. 2016:12:e1004762.

Glasser MF, Sotiropoulos SN, Wilson JA, Coalson TS, Fischl B, Andersson JL, Xu J, Jbabdi S, Webster M, Polimeni JR et al. The minimal preprocessing pipelines for the Human Connectome Project. *NeuroImage*. 2013:80:105–124.

Glasser MF, Coalson TS, Robinson EC, Hacker CD, Harwell J, Yacoub E, Ugurbil K, Andersson J, Beckmann CF, Jenkinson M et al. A multimodal parcellation of human cerebral cortex. *Nature*. 2016a:536:171–178.

Glasser MF, Smith SM, Marcus DS, Andersson JL, Auerbach EJ, Behrens TE, Coalson TS, Harms MP, Jenkinson M, Moeller S et al. The Human Connectome Project's neuroimaging approach. *Nat Neurosci*. 2016b:19:1175–1187.

Griffanti L, Salimi-Khorshidi G, Beckmann CF, Auerbach EJ, Douaud G, Sexton CE, Zsoldos E, Ebmeier KP, Filippini N, Mackay CE et al. ICA-based artefact removal and accelerated fMRI acquisition for improved resting state network imaging. *NeuroImage*. 2014:95:232–247.

Hackett TA, Stepniewska I, Kaas JH. Prefrontal connections of the parabelt auditory cortex in macaque monkeys. *Brain Res*. 1999:817:45–58.

Hackett TA, Preuss TM, Kaas JH. Architectonic identification of the core region in auditory cortex of macaques, chimpanzees, and humans. *J Comp Neurol*. 2001:441:197–222.

Hasselmo ME, Rolls ET, Baylis GC. The role of expression and identity in the face-selective responses of neurons in the temporal visual cortex of the monkey. *Behav Brain Res*. 1989a:32:203–218.

Hasselmo ME, Rolls ET, Baylis GC, Nalwa V. Object-centred encoding by face-selective neurons in the cortex in the superior temporal sulcus of the monkey. *Exp Brain Res*. 1989b:75:417–429.

van der Heijden K, Rauschecker JP, de Gelder B, Formisano E. Cortical mechanisms of spatial hearing. *Nat Rev Neurosci*. 2019:20:609–623.

Hornak J, Rolls ET, Wade D. Face and voice expression identification in patients with emotional and behavioural changes following ventral frontal lobe damage. *Neuropsychologia*. 1996:34:247–261.

Hornak J, Bramham J, Rolls ET, Morris RG, O'Doherty J, Bullock PR, Polkey CE. Changes in emotion after circumscribed surgical lesions of the orbitofrontal and cingulate cortices. *Brain*. 2003:126:1691–1712.

Huang C-C, Rolls ET, Hsu C-CH, Feng J, Lin C-P. Extensive cortical connectivity of the human hippocampal memory system: beyond the "what" and "where" dual-stream model. *Cereb Cortex*. 2021:31:4652–4669.

Huang CC, Rolls ET, Feng J, Lin CP. An extended Human Connectome Project multimodal parcellation atlas of the human cortex and subcortical areas. *Brain Struct Funct*. 2022:227:763–778.

Jeurissen B, Tournier JD, Dhollander T, Connelly A, Sijbers J. Multi-tissue constrained spherical deconvolution for improved analysis of multi-shell diffusion MRI data. *NeuroImage*. 2014:103:411–426.

Kaas JH, Hackett TA. 'What' and 'where' processing in auditory cortex. *Nat Neurosci*. 1999:2:1045–1047.

Kaas JH, Hackett TA. Subdivisions of auditory cortex and processing streams in primates. *Proc Natl Acad Sci U S A*. 2000:97:11793–11799.

Karabanov AN, Paine R, Chao CC, Schulze K, Scott B, Hallett M, Mishkin M. Participation of the classical speech areas in auditory long-term memory. *PLoS One*. 2015:10:e0119472.

Khandhadia AP, Murphy AP, Romanski LM, Bizley JK, Leopold DA. Audiovisual integration in macaque face patch neurons. *Curr Biol*. 2021:31:1826–1835 e1823.

Downloaded from https://academic.oup.com/cercor/article/33/10/6207/6960609 by University of Warwick user on 15 May 2023

Kikuchi Y, Horwitz B, Mishkin M, Rauschecker JP. Processing of harmonics in the lateral belt of macaque auditory cortex. *Front Neurosci*. 2014:8:204.

Kravitz DJ, Saleem KS, Baker CI, Ungerleider LG, Mishkin M. The ventral visual pathway: an expanded neural framework for the processing of object quality. *Trends Cogn Sci*. 2013:17: 26–49.

Kringelbach ML, Deco G. Brain states and transitions: insights from computational neuroscience. *Cell Rep*. 2020:32:108128.

Kringelbach ML, McIntosh AR, Ritter P, Jirsa VK, Deco G. The rediscovery of slowness: exploring the timing of cognition. *Trends Cogn Sci*. 2015:19:616–628.

Kusmierek P, Rauschecker JP. Functional specialization of medial auditory belt cortex in the alert rhesus monkey. *J Neurophysiol*. 2009:102:1606–1622.

Kuznetsov YA. *Elements of applied bifurcation theory*. New York: Springer Science and Business Media; 2013.

Leaver AM, Rauschecker JP. Functional topography of human auditory cortex. *J Neurosci*. 2016:36:1416–1428.

Lewis JW, Van Essen DC. Corticocortical connections of visual, sensorimotor, and multimodal processing areas in the parietal lobe of the macaque monkey. *J Comp Neurol*. 2000:428: 112–137.

Ma Q, Rolls ET, Huang C-C, Cheng W, Feng J. Extensive cortical functional connectivity of the human hippocampal memory system. *Cortex*. 2022:147:83–101.

Maier-Hein KH, Neher PF, Houde JC, Cote MA, Garyfallidis E, Zhong J, Chamberland M, Yeh FC, Lin YC, Ji Q et al. The challenge of mapping the human connectome based on diffusion tractography. *Nat Commun*. 2017:8:1349.

Maravita A, Romano D. The parietal lobe and tool use. *Handb Clin Neurol*. 2018:151:481–498.

Miller EK, Lundqvist M, Bastos AM. Working memory 2.0. *Neuron*. 2018:100:463–475.

Moerel M, De Martino F, Formisano E. An anatomical and functional topography of human auditory cortical areas. *Front Neurosci*. 2014:8:225.

Morel A, Garraghty PE, Kaas JH. Tonotopic organization, architectonic fields, and connections of auditory cortex in macaque monkeys. *J Comp Neurol*. 1993:335:437–459.

Munoz-Lopez M, Insausti R, Mohedano-Moriano A, Mishkin M, Saunders RC. Anatomical pathways for auditory memory II: information from rostral superior temporal gyrus to dorsolateral temporal pole and medial temporal cortex. *Front Neurosci*. 2015:9: 158.

Obleser J, Boecker H, Drzezga A, Haslinger B, Hennenlotter A, Roettinger M, Eulitz C, Rauschecker JP. Vowel sound extraction in anterior superior temporal cortex. *Hum Brain Mapp*. 2006:27: 562–571.

Ohashi H, Ostry DJ. Neural development of speech sensorimotor learning. *J Neurosci*. 2021:41:4023–4035.

Pandya DN. Anatomy of the auditory cortex. *Rev Neurol (Paris)*. 1995:151:486–494.

Passingham RE. *Understanding the prefrontal cortex: selective advantage, connectivity and neural operations*. Oxford: Oxford University Press; 2021.

Perrett DI, Rolls ET, Caan W. Temporal lobe cells of the monkey with visual responses selective for faces. *Neurosci Lett*. 1979:S3: S358.

Perrett DI, Rolls ET, Caan W. Visual neurons responsive to faces in the monkey temporal cortex. *Exp Brain Res*. 1982:47:329–342.

Perrett D, Mistlin A, Chitty A. Visual neurons responsive to faces. *Trends Neurosci*. 1987:10:358–364.

Petkov CI, Kikuchi Y, Milne AE, Mishkin M, Rauschecker JP, Logothetis NK. Different forms of effective connectivity in primate frontotemporal pathways. *Nat Commun*. 2015:6:6000.

Petrides M, Pandya DN. Comparative cytoarchitectonic analysis of the human and the macaque ventrolateral prefrontal cortex and corticocortical connection patterns in the monkey. *Eur J Neurosci*. 2002:16:291–310.

Petrides M, Pandya DN. Distinct parietal and temporal pathways to the homologues of Broca's area in the monkey. *PLoS Biol*. 2009:7:e1000170.

Pitcher D, Ungerleider LG. Evidence for a third visual pathway specialized for social perception. *Trends Cogn Sci*. 2021:25:100–110.

Pitcher D, Ianni G, Ungerleider LG. A functional dissociation of face-, body- and scene-selective brain areas based on their response to moving and static stimuli. *Sci Rep*. 2019:9:8242.

Plakke B, Romanski LM. Auditory connections and functions of prefrontal cortex. *Front Neurosci*. 2014:8:199.

Poremba A, Saunders RC, Crane AM, Cook M, Sokoloff L, Mishkin M. Functional mapping of the primate auditory system. *Science*. 2003:299:568–572.

Power JD, Cohen AL, Nelson SM, Wig GS, Barnes KA, Church JA, Vogel AC, Laumann TO, Miezin FM, Schlaggar BL et al. Functional network organization of the human brain. *Neuron*. 2011:72:665–678.

Rauschecker JP. Parallel processing in the auditory cortex of primates. *Audiol Neurootol*. 1998a:3:86–103.

Rauschecker JP. Cortical processing of complex sounds. *Curr Opin Neurobiol*. 1998b:8:516–521.

Rauschecker JP. An expanded role for the dorsal auditory pathway in sensorimotor control and integration. *Hear Res*. 2011:271:16–25.

Rauschecker JP. Ventral and dorsal streams in the evolution of speech and language. *Front Evol Neurosci*. 2012:4:7.

Rauschecker JP. Auditory cortex. *Reference Module in Neuroscience and Biobehavioral Psychology Brain Mapping*. 2015:2:299–304.

Rauschecker JP. Where, when, and how: are they all sensorimotor? Towards a unified view of the dorsal pathway in vision and audition. *Cortex*. 2018a:98:262–268.

Rauschecker JP. Where did language come from? Precursor mechanisms in nonhuman primates. *Curr Opin Behav Sci*. 2018b:21: 195–204.

Rauschecker JP, Scott SK. Maps and streams in the auditory cortex: nonhuman primates illuminate human speech processing. *Nat Neurosci*. 2009:12:718–724.

Rauschecker JP, Tian B. Mechanisms and streams for processing of "what" and "where" in auditory cortex. *Proc Natl Acad Sci U S A*. 2000:97:11800–11806.

Rauschecker JP, Tian B, Hauser M. Processing of complex sounds in the macaque nonprimary auditory cortex. *Science*. 1995:268: 111–114.

Rauschecker JP, Tian B, Pons T, Mishkin M. Serial and parallel processing in rhesus monkey auditory cortex. *J Comp Neurol*. 1997:382:89–103.

Razi A, Seghier ML, Zhou Y, McColgan P, Zeidman P, Park HJ, Sporns O, Rees G, Friston KJ. Large-scale DCMs for resting-state fMRI. *Netw Neurosci*. 2017:1:222–241.

Rilling JK, Glasser MF, Jbabdi S, Andersson J, Preuss TM. Continuity, divergence, and the evolution of brain language pathways. *Front Evol Neurosci*. 2011:3:11.

Rolls ET. Neurons in the cortex of the temporal lobe and in the amygdala of the monkey with responses selective for faces. *Hum Neurobiol*. 1984:3:209–222.

Rolls ET. Functions of the primate temporal lobe cortical visual areas in invariant visual object and face recognition. *Neuron*. 2000:27: 205–218.

Downloaded from https://academic.oup.com/cercor/article/33/10/6207/6960609 by University of Warwick user on 15 May 2023

Rolls ET. *Emotion and decision-making explained*. Oxford: Oxford University Press; 2014.
Rolls ET. Neural computations underlying phenomenal consciousness: a higher order syntactic thought theory. *Frontiers in Psychology (Consciousness Research)*. 2020:11:655.
Rolls ET. A neuroscience levels of explanation approach to the mind and the brain. *Front Comput Neurosci*. 2021a:15:649679.
Rolls ET. Mind causality: a computational neuroscience approach. *Front Comput Neurosci*. 2021b:15:70505.
Rolls ET. *Brain computations: what and how*. Oxford: Oxford University Press; 2021c.
Rolls ET. The hippocampus, ventromedial prefrontal cortex, and episodic and semantic memory. *Prog Neurobiol*. 2022a:217:102334.
Rolls ET. Hippocampal spatial view cells for memory and navigation, and their underlying connectivity in humans. *Hippocampus*. 2022b. https://doi.org/10.1002/hipo.23467.
Rolls ET. *Emotion, motivation, decision-making, the orbitofrontal cortex and the amygdala*; 2023a.
Rolls ET. *Brain computations and connectivity*. Oxford: Oxford University Press; 2023b.
Rolls ET, Treves A. The neuronal encoding of information in the brain. *Prog Neurobiol*. 2011:95:448–490.
Rolls ET, Hornak J, Wade D, McGrath J. Emotion-related learning in patients with social and emotional changes associated with frontal lobe damage. *J Neurol Neurosurg Psychiatry*. 1994:57:1518–1524.
Rolls ET, Treves A, Tovee MJ. The representational capacity of the distributed encoding of information provided by populations of neurons in the primate temporal visual cortex. *Exp Brain Res*. 1997a:114:177–185.
Rolls ET, Treves A, Tovee MJ, Panzeri S. Information in the neuronal representation of individual stimuli in the primate temporal visual cortex. *J Comput Neurosci*. 1997b:4:309–333.
Rolls ET, Critchley HD, Browning AS, Inoue K. Face-selective and auditory neurons in the primate orbitofrontal cortex. *Exp Brain Res*. 2006:170(1):74–87.
Rolls ET, Deco G, Huang C-C, Feng J. Prefrontal and somatosensory-motor cortex effective connectivity in humans. *Cereb Cortex*. 2022a. https://doi.org/10.1093/cercor/bhac391.
Rolls ET, Deco G, Huang C-C, Feng J. Multiple cortical visual streams in humans. *Cereb Cortex*. 2022b. https://doi.org/10.1093/cercor/bhac276.
Rolls ET, Deco G, Huang C-C, Feng J. Human amygdala compared to orbitofrontal cortex connectivity, and emotion. *Prog Neurobiol*. 2022c:220:102385.
Rolls ET, Deco G, Huang C-C, Feng J. The human posterior parietal cortex: effective connectome, and its relation to function. *Cereb Cortex*. 2022d. https://doi.org/10.1093/cercor/bhac266.
Rolls ET, Deco G, Huang C-C, Feng J. The human language effective connectome. *NeuroImage*. 2022e:258:119352.
Rolls ET, Deco G, Huang CC, Feng J. The effective connectivity of the human hippocampal memory system. *Cereb Cortex*. 2022f:32:3706–3725.
Rolls ET, Deco G, Huang CC, Feng J. The human orbitofrontal cortex, vmPFC, and anterior cingulate cortex effective connectome: emotion, memory, and action. *Cereb Cortex*. 2022g. https://doi.org/10.1093/cercor/bhac070.
Rolls ET, Wirth S, Deco G, Huang C-C, Feng J. The human posterior cingulate, retrosplenial and medial parietal cortex effective connectome, and implications for memory and navigation. *Hum Brain Mapp*. 2022h. https://doi.org/10.1002/hbm.26089.
Romanski LM, Tian B, Fritz J, Mishkin M, Goldman-Rakic PS, Rauschecker JP. Dual streams of auditory afferents target multiple domains in the primate orbitofrontal cortex. *Nat Neurosci*. 1999:2:1131–1136.
Romanski LM, Tian B, Fritz JB, Mishkin M, Goldman-Rakic PS, Rauschecker JP. Reply to What, 'where' and 'how' in auditory cortex. *Nat Neurosci*. 2000:3:966.
Salimi-Khorshidi G, Douaud G, Beckmann CF, Glasser MF, Griffanti L, Smith SM. Automatic denoising of functional MRI data: combining independent component analysis and hierarchical fusion of classifiers. *NeuroImage*. 2014:90:449–468.
Satterthwaite TD, Elliott MA, Gerraty RT, Ruparel K, Loughead J, Calkins ME, Eickhoff SB, Hakonarson H, Gur RC, Gur RE et al. An improved framework for confound regression and filtering for control of motion artifact in the preprocessing of resting-state functional connectivity data. *NeuroImage*. 2013:64:240–256.
Scheirer J, Ray WS, Hare N. The analysis of ranked data derived from completely randomized factorial designs. *Biometrics*. 1976:32:429–434.
Schurz M, Tholen MG, Perner J, Mars RB, Sallet J. Specifying the brain anatomy underlying temporo-parietal junction activations for theory of mind: a review using probabilistic atlases from different imaging modalities. *Hum Brain Mapp*. 2017:38:4788–4805.
Scott BH, Mishkin M. Auditory short-term memory in the primate auditory cortex. *Brain Res*. 2016:1640:264–277.
Scott BH, Mishkin M, Yin P. Neural correlates of auditory short-term memory in rostral superior temporal cortex. *Curr Biol*. 2014:24:2767–2775.
Scott BH, Leccese PA, Saleem KS, Kikuchi Y, Mullarkey MP, Fukushima M, Mishkin M, Saunders RC. Intrinsic connections of the Core auditory cortical regions and rostral Supratemporal plane in the macaque monkey. *Cereb Cortex*. 2017:27:809–840.
Seyfarth RM, Cheney DL. Production, usage, and comprehension in animal vocalizations. *Brain Lang*. 2010:115:92–100.
Sinha N. 2022. *Non-parametric alternative of 2-way ANOVA (ScheirerRayHare) MATLAB central file exchange*: https://www.mathworks.com/matlabcentral/fileexchange/96399-non-parametric-alternative-of-96392-way-anova-scheirerrayhare.
Skeide MA, Friederici AD. The ontogeny of the cortical language network. *Nat Rev Neurosci*. 2016:17:323–332.
Smith SM. Fast robust automated brain extraction. *Hum Brain Mapp*. 2002:17:143–155.
Smith SM, Beckmann CF, Andersson J, Auerbach EJ, Bijsterbosch J, Douaud G, Duff E, Feinberg DA, Griffanti L, Harms MP et al. Resting-state fMRI in the Human Connectome Project. *NeuroImage*. 2013:80:144–168.
Smith RE, Tournier JD, Calamante F, Connelly A. SIFT2: enabling dense quantitative assessment of brain white matter connectivity using streamlines tractography. *NeuroImage*. 2015:119:338–351.
Spierer L, Bellmann-Thiran A, Maeder P, Murray MM, Clarke S. Hemispheric competence for auditory spatial representation. *Brain*. 2009:132:1953–1966.
Sulpizio V, Galati G, Fattori P, Galletti C, Pitzalis S. A common neural substrate for processing scenes and egomotion-compatible visual motion. *Brain Struct Funct*. 2020:225:2091–2110.
Tian B, Reser D, Durham A, Kustov A, Rauschecker JP. Functional specialization in rhesus monkey auditory cortex. *Science*. 2001:292:290–293.

Downloaded from https://academic.oup.com/cercor/article/33/10/6207/6960609 by University of Warwick user on 15 May 2023

Valdes-Sosa PA, Roebroeck A, Daunizeau J, Friston K. Effective connectivity: influence, causality and biophysical modeling. *NeuroImage*. 2011:58:339–361.

Van Essen DC, Smith SM, Barch DM, Behrens TE, Yacoub E, Ugurbil K, WU-MH C. The WU-Minn Human Connectome Project: an overview. *NeuroImage*. 2013:80:62–79.

Van Essen DC, Glasser MF. Parcellating cerebral cortex: how invasive animal studies inform noninvasive mapmaking in humans. *Neuron*. 2018:99:640–663.

Yokoyama C, Autio JA, Ikeda T, Sallet J, Mars RB, Van Essen DC, Glasser MF, Sadato N, Hayashi T. Comparative connectomics of the primate social brain. *NeuroImage*. 2021:245:118693.

Downloaded from https://academic.oup.com/cercor/article/33/10/6207/6960609 by University of Warwick user on 15 May 2023